An experimental study of stylolite formation

by
Ola Kaas Eriksen
Physics of Geological Processes
Department of Physics
University of Oslo
Norway

Thesis submitted for the degree
Master of Science

October 2008

Abstract

Stylolites are features of localized dissolution in sedimentary rocks. They are planes oriented normal to the compaction direction and have a rough and often teeth-like surface structure. The vertical spacing of individual stylolite planes are often constant within one rock sample or outcrop. There is no general agreement on how these rough planes of localized compaction form. We present experimental result in this thesis that suggests that the characteristic diffusion length of solute is important for both the localization process and the vertical spacing of individual stylolite planes. We have done experiments where granular systems are compacting by pressure solution and by mechanical compaction. The results from the mechanically compacted experiment shows a clear anticrack formation around an inclusion in the compacting matrix. The results from the experiments compacted by pressure solution on the other hand show no localized compaction around the inclusion at all. There is no anticrack. The system develops spontaneously a "compaction band" structure oriented normal to the compaction direction. The spacing between the bands in this band structure is 1-2 mm, which is consistent with stylolite spacing in calcitic rock of 20-150 cm, assuming that the precipitation rate determines the characteristic diffusion length. We know that individual stylolite planes will approach each other with up to 10 cm because of dissolution of rock on the stylolite surface. Our estimate of stylolite spacing fits observed spacings surprisingly well. The localization in our experiments is clearly not triggered by the inclusion. We propose that the mechanism for localization is initial porosity variations and/or variations in clay concentrations combined with a long characteristic diffusion length, which also controls the spacing of individual stylolite planes. We also do roughening experiments where polished sintered salt blocks stacked on top of each other in a cylinder, and stressed in the direction normal to the surface. The results from these experiments propose a roughening with a wavelength of 2-4 mm.

Acknowledgment

First off all I would like to thank my main supervisor Dag Kristian Dysthe for his help and support during my period at PGP. His creativity and expertise as an experimentalist has helped me in the process of developing a good experimental study. The discussions with him have always given me ideas and motivation for further development. He has always been supportive and invited me over to his home for discussions after his kids bedtime more than once when things have been hectic. Thank you Dag!
I would also like to thank my three other supervisors, Francois Renard, Joachim Mathiesen and Espen Jettestuen. Thank you Francois for fruitful conversation, both when you have visited us at PGP and when you have invited us to France. Thank you Joachim for your good explanations. You have always given my a good explanation when I have dropped by your office with something I do not understand. And thank you Espen for helping me when there have been trouble with the image analysis, and other Matlab trouble. I could not have done it without your help. Thank you!
Thank you Olav Gundersen for help with lab equipment. I would like to thank all the people at PGP for a good learning and social environment. Thank you Luiza for some good discussions about confusing papers. Thank you Anders and Simon for discussions about everything from physics to skiing. Thanks to all the other master students, especially Yngve and Munib. We have supported each other the two years we have studied together at PGP. Thank you Kirsten for trying to improve my English. And thanks to all my friend outside PGP.
Nobody deserves a thank you more than my parents Claus Petter Eriksen and Kristin Kaas. They have given me all possible support through my whole, life including my time at the University. They have given me both moral support and supported me with practical things as food and laundry during my studies. I would also like to thank my sister Marie for her support. And last I will thank my girlfriend Lene for her support and understanding in periods when studies have occupied all my time.

Contents

Chapter 1

Introduction

When marine organisms die, the chalk-rich parts of the organisms with bone structure and/or shells, such as fish and mussels, fall down to the sea floor as sediments. As more and more of these organically derived sediments fall down, they slowly get buried on the sea floor. The buried volume of sediment and water is exposed to the stresses from the surrounding sediments, σ_{ij}, and the fluid pressure, P_f. These stresses will cause compaction and expulsion of pore fluid. The main compaction will be in the direction of the effective deviatoric stress $\sigma_{i_m i_m} - \frac{1}{3}\sum_i \sigma_{ii} - P_f$. This is normally in the vertical direction because of the weight of the overlying sediments, but tectonic stresses can cause main compaction in other directions as well. Pressure solution, in addition to cataclasis, grain sliding, and plastic deformation, is one of the important processes in this compaction [8]. Pressure solution is a very slow process, and the compaction of these sediments may take thousands, or even up to millions of years. After all these years of compaction the sediments have become rock. Sedimentary rocks are found all over the world and there are very often patterns made out of darker lines visible on the rock. The lines are cross sections of planar structures that go through the rock. These planes are often a product of localized dissolution in the pressure solution process. Pressure solution will be explained later. The shape of the lines vary; they can be flat, wavy, or have a teeth-like structure with sharp teeth walls that are oriented normal to the main direction of the line. The lines with teeth structure are called stylolites. In figure 1.1 we see both the dark line with teeth structure and the three dimensional rough surface that the line is a cross section of. Stylolites are fairly commonly observed, and the best places are often on buildings, bridges etc. where the rock surface is smooth and often polished. Even though they are such a common feature, there is no general agreement on the how stylolites form.

Stylolite formation is not a complete mystery, there is some things that are commonly known;
They are believed to be a product of compaction where the stylolite planes form normal to the compaction direction [15]. Pressure solution, which is believed to be the important process in their formation, has occured faster on the stylolite surface, meaning that more material has been dissolved on the stylolite than in the bulk rock [20]. Stylolites are usually covered with clay particles and they have a higher concentration of insoluble particles than the bulk rock [20]. Clay is believed to be essential in the localization of dissolution we see on these planes [4]. The amount of clay in the bulk rock is also believed to be an important factor for how rough the stylolites are. The roughness decreases with increasing clay content, and the "stylolites are usually flat when the clay content in the bulk rock is as high as 50 percent" (noe francois sa en gang). Flat stylolites are called dissolution cleavages or dissolution seams. Heterogeneities in the compacting rock, like large rigid objects (much larger than the grain size) or soft spots, and insoluble particles in the bulk rock, are also factors believed to be important for how the stylolites grow [9].
Many observations of stylolites have been made. Where they are found, their different shapes and their different particles content have been studied [20][17][12]. Simulations of stylolite formation have also been done [15][10][6][20][14]. There are many studies of stylolites, but there is a lack of publications on experiments attempting to reproduce them. This suggests that stylolites and other features of localized dissolution is problematic to reproduce in the laboratory.

1.1 Motivation

Natural phenomena that are not yet understood have motivated many scientists throughout history. When we see a pattern that we are not able to explain, it is in our nature to investigate. Similarly my motivation for this study is to gain knowledge and understanding of stylolites and the processes that are important in their formation. An investigation of one problem is very often linked to other well or less well understood problems. Compaction is an important process in many naturally ocuring settings, and it is therefore important to understand. But we cannot claim to have a full understanding of compaction when there are features, such as stylolites, linked to the process that we do not understand. So to understand compaction of sedimentary

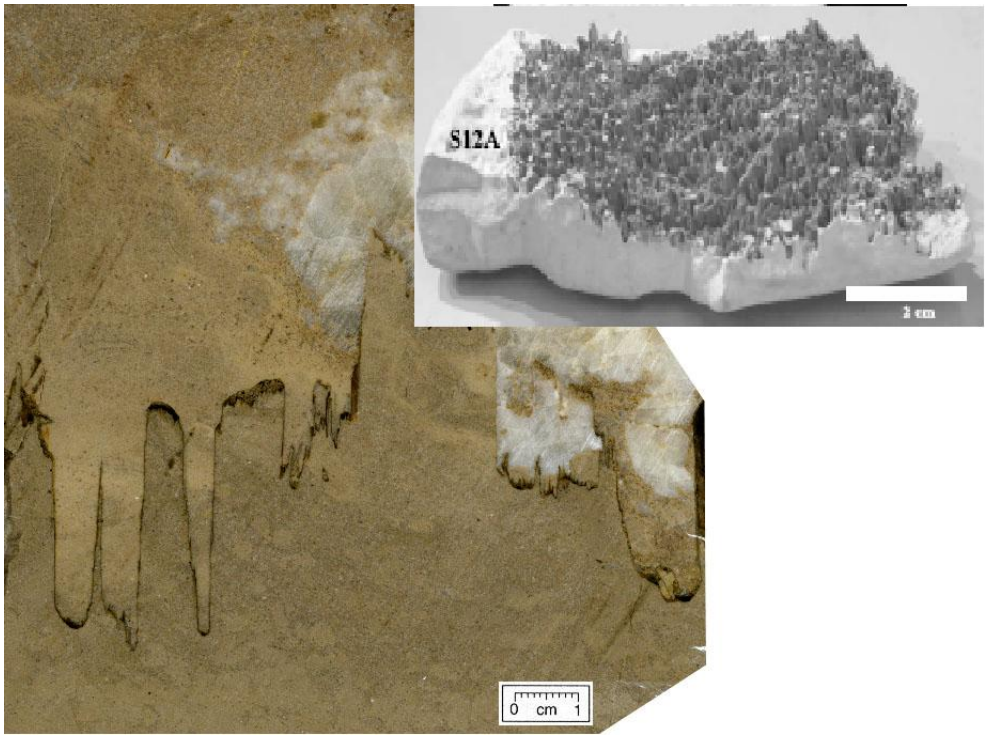

Figure 1.1: To the left is a stylolite as normally observed, in cross-section. It is a thin line with a rough teeth structure. In the right photo the rock that is covering the stylolite surface has been removed and we see the rough three dimensional surface of the stylolite The images are taken from [20] and [1].

basins better, it is important to understand why and how these localization features form. A greater understanding of the localization process can be helpful in other settings in addition to this particular compaction problem.

1.2 Experimental approach

When there is a phenomenon that is not understood, one way of gaining knowledge and understanding is to do experiments. A good experimental study is, together with theory and simulations, necessary to get a full understanding of a problem. The ideal scenario is where every experimental result is explained by theory and every theory is backed up by experimental results. In the stylolite study there are a lack of experimental results to back up the theories and simulations on the subject. There is also some disagreement between the different theories, so an experimental study with results that can be compared to the different theories is needed.
An experimental study is often very time demanding and you often work in a loop where the results from the first experiments are in the form of more questions and ideas for improvements or totally new experiments. In order to get to a conclusion, you often have to follow this loop several times. The starting point of an experimental study is important and difficult. The phenomena we want to investigate is complex and there are several variables that might play an important role. It is therefore important to take the problem apart and find specific questions on smaller parts of the problem. For instance, in this case the question "how do stylolites form?" is a bit too big and general to answer. Instead, we have to dig in to the problem and ask more specific questions; For example, how is the compaction evolving around an inclusion in the compacting material? is a more specific question that is easier to study experimentally. By finding answers to smaller questions like this, the bigger picture of how the stylolites form might come clear.
When you have a specific question and a specific goal for the experimental study, you must find a physical system that is appropriate. Often, especially when you study phenomena linked to geological processes, you must choose a model that has totally different length and time scales than the physical system where you find the phenomenon in nature. So first, you must find out in what systems the phenomenon is observed in nature, and then find a model that fits in the laboratory and that will give results in a reasonable time.
Experiments linked to geological problems often require that you use a model material instead of rocks, which often require too long time and too high

temperatures and stresses. Especially in this problem, where the deformation process is linked to dissolution. Rocks do not dissolve very fast in water. When the model material is chosen, the-set up and measurements need to be sorted out. You need to know what you want to measure, and how you are going to measure it, in order to make a set-up that allows these measurements. There is often a battle between two and three dimensional experiments. The three-dimensional experiments are often more similar to the natural system you want to simulate, but there are often a limited number of measurements possible. A two-dimensional measurement often allows measurements not possible in a three dimensional set-up, but it is often less similar to the natural system due to the imposed restriction in one dimension.
A good analysis of the results from an experiment is always required. Some results need a sophisticated analysis tool, while others are simpler to analyse. It is important to have a good analysis tool that gives you the information you need from the experiments. In our case, it was important to develop a good image analysis tool. Depending on your measurements, you need a good analysis tool to analyse the measurements and get the results you need. If the measurement are a series of photos you need a good image analysis tool to acquire the information you need.

1.3 Questions

In this experimental study, the main question is how do stylolites grow? As mentioned, the motivation is to obtain more knowledge about stylolites and their formation. The problem is then divided into three main questions.
The first question is: why is there a localization of dissolution on the stylolite surface? This is also a general question and we end up asking; what happens around an inclusion (soft or hard) lying in a compacting porous material? Will stress concentrations around the inclusion lead to localization of compaction and then an anticrack (The anticrack model is explained in the theory chapter)?
The second main question is; why do the stylolites have such a rough and teeth-like structure? Examining this question from another perspective, it could be rewritten as: what happens to a pre existing flat surface when the material is compacted further?
The third question involves the relationship between individual stylolite planes. Individual stylolite planes often have a more or less constant spacing [16]. What determines this spacing?

Chapter 2

Observations, theory and simulations

There are several theories and simulations on stylolite growth. The different theories are not in total agreement. The different theories have different mechanisms for localization of compaction. Stress concentrations are important in all of them, but which processes lead to these stress concentrations vary. There are a couple of suggestions; pure mechanical (elastic response of the material around flaws in the matrix), and variation in viscosity due to concentration differences of catalyst minerals that enhance dissolution. There are also several theories about surface roughening.

2.1 Observations

Stylolites are observed in all sedimentary rocks but are most common in limestone. They are visible because of a high concentration of insoluble particles, mostly clay, on the stylolite surface. The stylolite surface is normal to the direction of the maximum compressive stress and they are used by geologists to determine the direction of the maximum compressive stress in regions where they are found [15]. The stylolites have a rough structure with teeth-like columns with side walls sometimes parallel to the direction of maximum compressive stress. Stylolite planes can have plane lengths of up to tens of meters, while the column height is typically from a couple of mm to a couple of cm [12]. There are also micro stylolites. These form in grain contacts and look like normal stylolites only much smaller. It is not known if the same processes are behind the formation of micro stylolites and normal stylolites [17]. The height of the stylolite columns are sometimes used as an estimate for the amount of rock dissolved on the stylolite surface, but

this is not believed to be a very accurate measure [20][15]. Measurements done by Renard et al. [20] show that the concentration of titanium, iron and phosphorus are 5 to 20 times higher in the stylolite than in the bulk rock. The interfaces where these measurements are done are 0,5 to 5 mm thick so the estimated thickness of the layer of rock dissolved is 2,5 to 100 mm. This thickness is comparable with the height of the stylolite teeth. There are however many factors that might affect this estimate, such as circulating fluids.

2.2 Pressure solution

As mentioned previously there are some disagreements in stylolite theory, but in all the theories pressure solution is an important process. When sediments are compacting under the sea floor there is water present. The water is a solvent for these chalk-rich sediments and the water will eventually be saturated. The saturated water fills the pore space surrounding the compacting sediments. The different components of the sediments have different solubility. Some of them do not dissolve in water at all. The solubility in water (grams of material that can be dissolved in 100 ml. water) is dependent on several variables. Many materials have a temperature dependent solubility, but locally the temperature in the compacting sediments is very constant. Stress is also affecting the solubility of compacting sediments. The solubility is stress dependent because stress changes the chemical potential of the solid phase of the compacting material. The chemical potential of the solid grains will increase in areas of their surface with high stress. A solution is saturated when there is a balance in chemical potential between the surface of the solid grains and the surrounding solution. When the chemical potential of the solid grains increases locally, the solution in contact with this area has to dissolve more material to be in local chemical equilibrium (to be saturated). This solution will now have a higher concentration of dissolved material than the rest of the saturated solution that is not in contact with any highly stressed grains. There will then be a difference in chemical potential in the solution and this difference will drive the diffusion of dissolved material away from the stressed area. When the dissolved material has diffused toward areas with less stress, the solution in these areas will be oversaturated. The dissolved material will then precipitate in these low stress regions. When material is dissolving in the grain contacts and is precipitated in the pore space, we get a volume reduction due to a reduction in porosity. This compaction process is called chemical compaction or pressure solution and is a very slow process.

Figure 2.1: Thin sections from St. Peter sandstone, St. Charles Co., Missouri. a) shows clay free sandstone and b) shows clay bearing sandstone collected just a few cm below a). We can clearly see the effect the clay had on the compaction of this sandstone. Picture taken from Weyl [22].

What process limits the speed of the pressure solution varies. It can be limited by how fast material dissolves, by how fast material diffuses away from the contacts, or how fast material precipitates. No matter what controls the speed, it is a slow process. In sedimentary basins where quartz-rich sediments are compacting, precipitation is limiting the compaction between 3 and 5 km depth. Below 5 km depth, diffusion is the limiting factor. Above 3 km depth pressure solution is so slow its rate can be neglected [8]. In compaction of salt aggregates at room temperatures, diffusion is the limiting factor [8].

For pressure solution to be possible there has to be water present. There has to be a thin film of water trapped between the grains. There is no pressure solution in healed grain contacts with no water film. In grain contacts with stresses above the limit for plastic deformation, material can dissolve from the plastically flowing solid into the surrounding water. Healed contacts will be discussed in the next section. The presence of clay is also believed to affect the pressure solution process. It is known that clay increases the speed of the process and experiments done with compaction of salt clearly shows this effect [19]. Why is clay a catalyst in the pressure solution process? It is believed both to increase dissolution speed and also speed up the diffusion because it props up grain contacts. Clay might also have an effect on the characteristic diffusion length. If the grains are covered with clay and there are no clean surface to precipitate on, the precipitation goes slower and the material diffuses farther before it precipitates. Thus the presence of clay is important in several ways.

In summary, some of the important factors in the pressure solution process are stress, water and clay. Stress drives the compaction. With no stress there will be no grain contacts where more material can dissolve. The higher stress the higher compaction speed. Water is absolutely necessary as solute and diffusion medium, and clay speeds up the whole process considerably.

2.3 Pressure solution vs healing of grain contacts

As mentioned it is absolutely necessary to have a film of water between the grain contacts to have pressure solution. The exception is in grain contacts with very small areas or at great depths where stresses are above the limit of plastic deformation. In these contacts, material can dissolve without the water film present. When sediments are buried under the sea floor, there is water between every grain. As the sediments get more and more buried and the stresses grow, some of the contacts actually heal. In these contacts, the direction of the crystal structure in the grains is lying in a way where it is more energy efficient to grow together to be one grain rather than having two surfaces with a water film in-between. In some grain contacts in the compacting material there will be a film with water and in others there will be a healing process whereby the two grains become one. It is a matter of what has lowest energy; The surface energy of the two grain surfaces or the energy barrier to grow a crystal structure between the two grains. Therefore the factor deciding whether there will be healed contacts or two grains with a water film in-between is the relative direction of the crystal structure of the two grains. If the crystal lattices of the two grains have the same direction, the energy barrier to grow together is small and they will probably grow together. If the deviation of direction is large the energy barrier is big and it is likely more efficient to have two surfaces with their given surface energy. How smooth and flawless the surfaces are will also affect the lowest energy state. In a compacting material, there is a battle between these two processes, resulting in some healed contacts and some contacts with a water film.

2.4 Localized compaction

2.4.1 The Anticrack model

The anticrack model suggests that solution surfaces or dissolution planes originate from stress concentrations, and propagate through the compacting

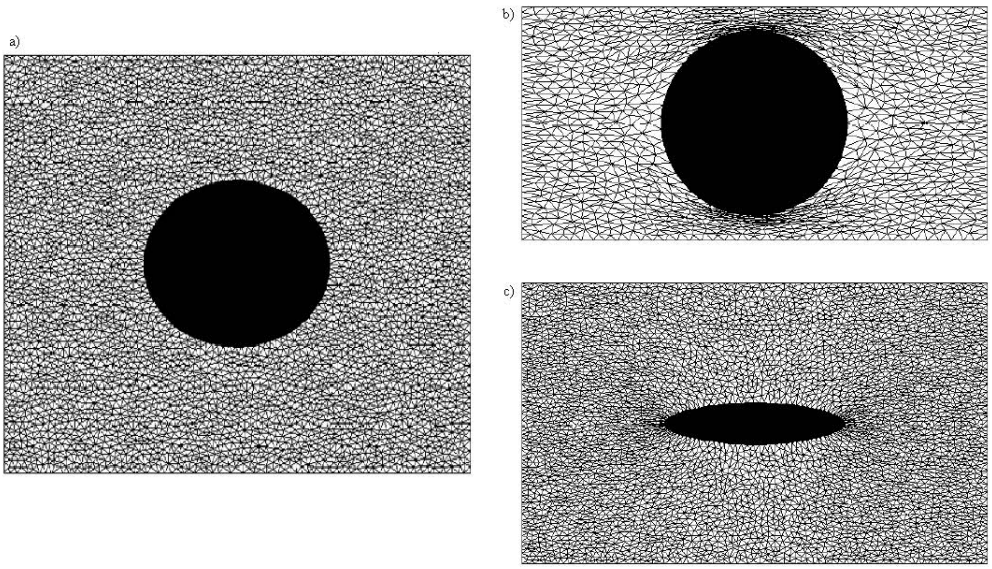

Figure 2.2: Compaction of a linearly elastic material around a hard and a soft inclusion. a) shows the initial system before compaction. b) shows the compaction around a hard inclusion and c) shows compaction around a soft inclusion. The finite element model used is made by Luiza Angheluta.

material as anticracks. When the material is compacting the stress and displacements fields are similar to those of an opening crack, but with a change of sign.
The anticrack model is a model where stress driven compaction is localized in stress concentrations around heterogeneities like rigid inclusions or soft spots in the compacting material. The stress concentration will cause local volume reduction that will propagate out from its origin in the direction normal to the stress direction as an anticrack.
In a compacting elastic material, stress concentrations will occrure around inclusions in the matrix because of the elastic response of the material. The stress will concentrate on the top and bottom of a hard inclusion and on the sides of a soft inclusion, see figure 2.2.

The anticrack model suggest that when the stress concentration have caused a local volume reduction, the stress concentration will move outward from the inclusion where it started. There will then be a plane of localized compaction propagating out from the inclusion in the direction normal to the compaction direction. The propagation of this plane will have similarities with the propagation of a tensile crack, only much slower, hence the name

anticrack. In a tensile crack the crack walls are moving away from each other. In the anticrack model they change the sign of this wall movement. This leads to a penetration of the two walls. To avoid this problem they assume that the penetrated volume of rock is dissolved by pressure solution. The anticrack will then grow in thickness as it grows in length.

2.4.2 Compaction bands

R. Katsman et al. [14] has modelled compaction of an elastic material using a spring network model. They look at compaction of a two-dimensional system where a thin lamina of material lying in the direction normal to the compaction direction is removed. This lamina is simulating an already formed compaction band. Removing a thin lamina like this will lead to internal stresses in the material that will persist for any remotely applied stress. They compare the stress field around this compaction band with the analytical solution of a similar problem solved by Eshelby, and the stress fields are very similar. The stress field around this compaction band shows large stresses concentrated around the tip of the compaction band. The compacting stress have a positive peak just outside the compaction band and a negative peak just on the inside. See figure 2.3. In a compacting system where a compaction band has formed, there will be stress concentrations just outside the band tip. The stress on the compaction band flanks on the other hand will be smaller than or similar to a remotely applied stress. Because the compaction is purely stress driven the compaction band will propagate in the direction normal to the maximum stress direction, and the width of the compaction band will not grow with further compaction. Thus there is a disagreement on the width of the compaction band or anticracks between Katsman et al. and Fletcher et al. The anticrack model uses the wall displacements of opening cracks just with a changed sign. This will lead to an interpenetration of the anticrack walls. This problem is solved by assuming that this material is removed by pressure solution. This way, the anticrack will get wider with further compaction.

2.4.3 Localized compaction in drinking straw set up

The compaction of solids is often heterogeneous. Many types of set-ups give a localization of compaction [18]. This could for instance be honeycomb two-dimensional cellular solids or packings of drinking straws. This type of set-ups shows a behaviour that first is elastic, by bending of the walls, then the compaction become localized when walls are starting to buckle. Where the first wall buckles it will grow a compaction band in the direction normal

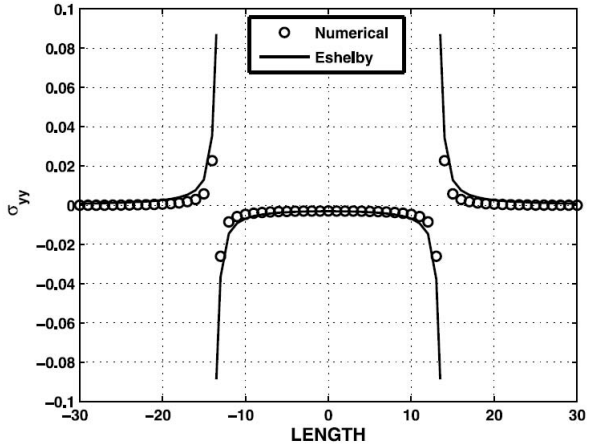

Figure 2.3: Plot of compacting stress along the compaction band. The length of the compaction band is 27. The agreement of the analytical solution of Eshelby and the result from the numerical model is convincing. The remotely applied stress is here 0. The figure is taken from Katsman et al. [14]

to the maximum compacting stress. This is similar to what the anticrack model predicts.
C. Poirier et al. [18] have studied compaction of drinking straws packings. There are three types of disorder that are believed to result in localization in a set-up of compacting drinking straws; 1) Disorder in a regular packing of formally identical straws because of small individual variations in the straws or the packing. 2) Introduction of drinking straws with different diameter in the system will lead to geometrical disorder. 3) Disorder in a regular packing of straws where some of the straws have a different composition and therefore a different strength.
The system studied by Poirier et al. is a regular packing of identical straws. The size of the cell the straws are packed is an integer ratio of the straw diameter in order to get a packing as crystalline as possible. The walls of the cell are coated with Teflon to remove wall effects. This way there are very little flaws in the packings of straws so any localization of compaction should come from individual variations of the straws.

The results from the experiments clearly shows a localization of compaction in bands randomly distributed in the system. There are a higher concentration of bands in the upper part of the cell because of wall friction. The geometry of the bands follow a power law; W^{ζ} with an exponent

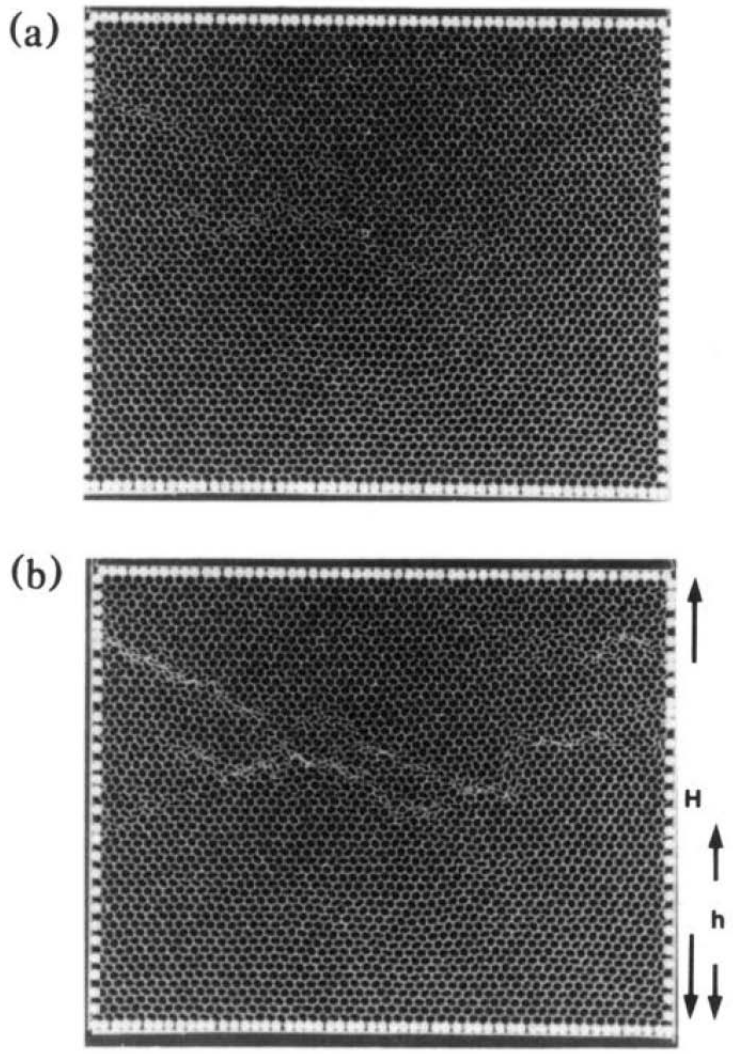

Figure 2.4: Two photos of two different stages in the compaction. In a) we see localized compaction in the form of clusters of flat straws. In b) we see The bands of compacted straws connecting. The figure is taken from Poirier et al. [18]

$\zeta = 0,73 \pm 0,07$. This is close to the exponent of opening cracks which is $\zeta = 0,7 \pm 0,07$ [18]. This is an interesting result for the debate between Fletcher et al. and Katsman et al. on weather the width of an anticrack or compaction band are growing or not.

2.4.4 Finite element modelling

Fueten et al. have made a finite element model that reproduce patterns very similar to the ones observed in nature. In the model they compact a two-component material consisting of quartz and mica. Quartz is the mineral that can dissolve in the surrounding solvent and mica is a catalyst in this process. There is a certain quartz to mica ratio that gives the highest dissolution rate and therefore the lowest viscosity. In mixtures with high concentrations of quartz, the dissolution will go slow because of the absence of the catalytic mica. In mica-rich regions the dissolution is slow because of low content of quartz to dissolve. The starting point for the simulation is a slab of material with a mica concentration much lower than the value that maximizes the dissolution rate (gives lowest viscosity). There are seeds distributed in the matrix that have a higher concentration of mica, but are still below the minimum viscosity value. The system is then stressed with a load in the vertical direction. Local dissolution is calculated from local stress and the mica content. The dissolved silica from the quartz, which is the only mobile component in the system, is evenly distributed throughout the volume with no real time scale or driving force, i.e. there is no real diffusion. When the system is stressed the less viscous seeds will dissolve more quartz than the bulk. This quartz is then removed leaving the seed even less viscous. The localized dissolution causes material to be removed from the seeds leading to stress concentrations near the tips of the seeds. These stress concentrations increase the dissolution and the length of the seam (growing from the initial seed) will increase, similarly to a propagating anticrack.

When compacted further, the seam will have a very high mica concentration and consequently a high viscosity. The regions above and below the seam are also very viscous because of all the quartz diffusing from the seed into these regions. The length of the seam is growing because of stress concentrations at the tip of the seam. This stress concentration has a fan shape, resulting in a fan shaped region with lower viscosity at the tip of the growing seam. When there is more than one initial seed, an overlap of these fan shaped regions will lead to a connection of the seams into one long seam that can have a wavy shape. When compacted further, the seams grow in thickness and the system develops more seams.

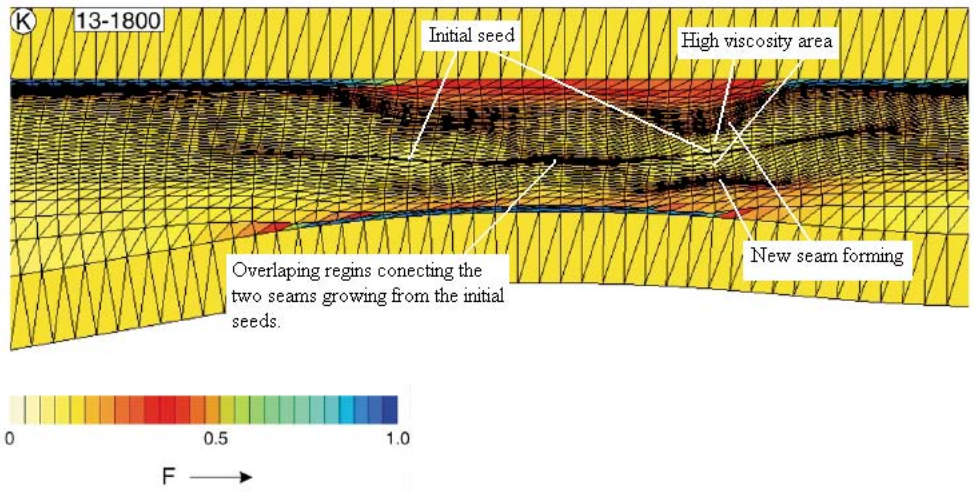

Figure 2.5: The system after the last step in the run. The system has two initial seeds connected with a thick seam. We can see new seams forming in areas above and below the initial seeds. The colour coding is the composition of the material, where one is 100 percent mica.

The localization process in this simulation is mainly caused by viscosity variations due to composition variations in the compacting rock. Regions where the ratio between the soluble material and catalyst is ideal, will have a lower viscosity. This will lead to stress concentrations and growing of dissolution seams. In essence, this model, which has no diffusion, is like a mechanical model with a positive feedback through the mica concentration and the stress concentration. In this model, the disolvable material is quartz and the catalyst is mica. In our experiment, the soluble material could be some kind of salt with clay as the catalyst.

2.5 Precipitation and spacing of stylolites

The spacing between stylolites is very often close to constant within the same sample or outcrop. The main transport mechanism of solute in the compacting rocks is believed to be diffusion. The spacing between the stylolites might therefore be linked to the characteristic diffusion length of this solute. This length will depend on the speed of diffusion, which again depend on gradients in chemical potential, and how fast the material is precipitating, which depends on the material, clay content and surface properties of the solid phase of the material. Enrique Merino et al. [16] have a theory where small porosity changes in the stressed rock will lead to that this small differences increases with positive feedback until collapse of the rock. The theory claims that in a region where the porosity is slightly higher the stress in the grain contacts will be slight higher as well. This will lead to a higher dissolution rate in this region. The solute will then diffuse in to an area that is less stressed. This is true, assuming that the characteristic diffusion length is so long that this area of less stress is not the pore space surrounding the highly stressed contacts but an area of the rock with less porosity. Thus the dissolved material is diffusing away from the porous region into a less porous region where it precipitates. This will lead to an even bigger difference in porosity and this process will speed up and continue until the highly porous region collapses. One initial region of high porosity will cause a region of low porosity in a certain distance, depending on diffusion length, away. This porosity minimum region will again lead to another porosity maximum on its other side. This way, the distances between the high porosity regions that will collapse and later become dissolution seams or stylolites become relatively constant. This spacing is dependent on how far dissolved material diffuses before it precipitates. It requires that this distance is greater than just out in the pore space next to the grain contact where it was dissolved. If that were the case, the porosity differences would even out. Therefore, it

is a question of whether a system with internal porosity changes is stable or not. It is believable that it is some critical characteristic diffusion length that decides whether the system is stable or not.

2.6 Roughening of flat surfaces

2.6.1 The Asoro-Tiller-Grinfeld instability

The Asoro-Tiller-Grindfeld instability is believed by some to be a roughening mechanism of stylolites [11]. It is an instability of a solid liquid interface exposed to a lateral stress. This interface will be unstable and roughen for an initial perturbation with wavelengths longer than the critical wavelength λ_c. In a set-up where you have a solid that is exposed to a lateral stress and have a wavy free surface with a fluid on top of it like in figure 2.6, the solid fluid interface is unstable for some wavelengths. The stress concentrations in the valleys of the solid is driving the instability. Material will dissolve here and precipitate on the peaks where there is less stress. When the peaks are growing, their radius of curvature is getting smaller and their surface energy will increase. This will lead to dissolution on the peaks and the interface will flatten out. Whether the flattening surface energy term or the stress concentration driven roughening term gives the lowest energy, is determined by the wavelength of the interface. There is a critical wavelength, and shorter wavelengths gives flattening and longer wavelengths give roughening. This model uses an instability where the stresses are lateral, parallel to the roughened interface. The direction of the maximum compressive stress in systems where we observe stylolites are always normal to the rough surface (the stylolite). Let us consider a system like the one in figure 2.6, only with another solid block on top of the liquid layer, where the side walls are fixed. An applied stress in the y direction will result in a stress in the x direction as well because of the Poisson ratio. We can assume that the stress in y direction is what drives the pressure solution and that the stress in x direction makes the surface unstable. Is it assumed that the Asoro-Tiller-Grindfeld instability, which considers a solid liquid interface, is reasonable to use because of the liquid film between the two solid blocks.

2.6.2 Noise driven roughening

Daniel Koehn et al. [15] have made a model where they simulate the roughening of an initial flat surface. The model consists of two solids separated

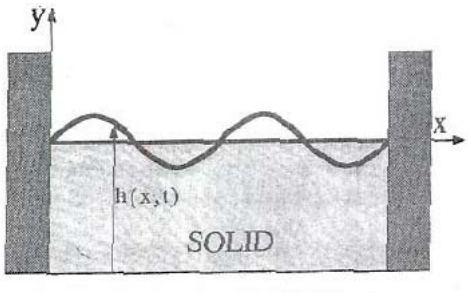

Figure 2.6: A solid exposed to a lateral stress. The wavy solid liquid interface in unstable for wavelengths longer than some critical wavelength. The figure is taken from Srolovitz [21]

by a flat interface. The solids consist of particles in a triangular lattice and they are connected with linear elastic springs. A constant displacement rate is applied to the system in the direction normal to the interface separating the two solids. Stresses will build up because the displacement and the fluid that was initially in equilibrium with the solid is becoming undersaturated. This will lead to dissolution of particles on the surface where the dissolution is limited to happen. In this model, transport of solute is not taken into account and the dissolved particles are assumed to diffuse out of the system and not precipitate anywhere. 5 percent of the particles in the system have a solubility of half the value of the rest of the particles. These particles will require twice the time to dissolve. Because of this difference in dissolution time the interface will roughen. When a slowly dissolving particle is reaching the interface, the interface will have one slowly dissolving particle on one side and a quickly dissolving particle on the other. The interface will then move in the direction of the quickly dissolving particle. The slowly dissolving particles are randomly distributed in the solids and this random noise is what causes the roughening.

In this model the material compacts because of pressure solution, but the dissolution is only allowed on the initially flat interface. This corresponds to a natural system where you have two solids where all the grain contacts have healed, and there are no fluid films between the grains. In this situation, there is only one interface where fluid is present, such as a crack, and that is where material can dissolve.
They present simulation data for system sizes of 0.4, 4 and 40 cm. The

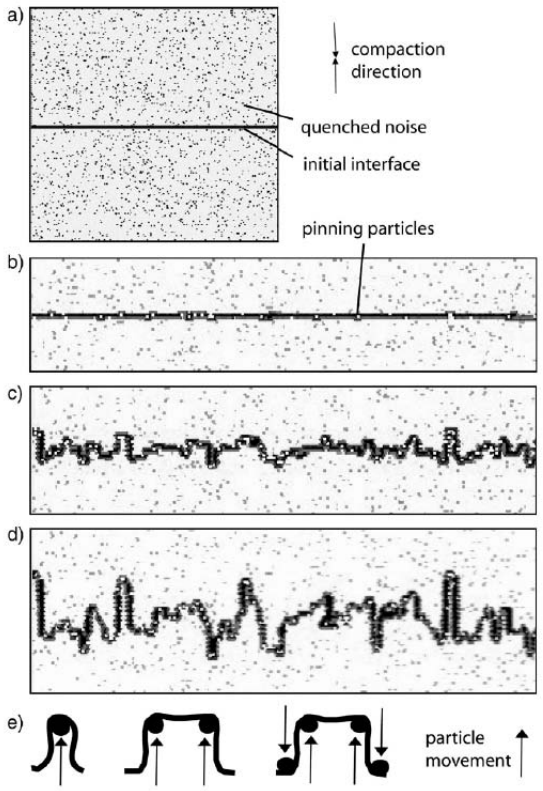

Figure 2.7: In figure a) we see the initial system with the flat interface and the randomly distributed slow dissolving particles. Figure b) to d) shows the evolution of the interface. The white dots are the slow dissolving particles that are pinning the interface. Figure e) shows the evolution of the interface during pinning. The figure is taken from the article by Koehn et al. [15]

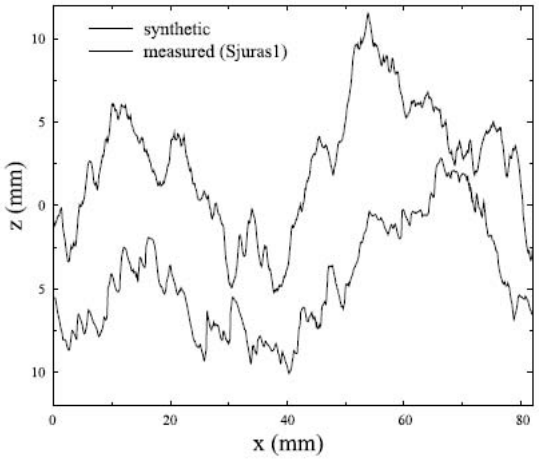

Figure 2.8: The upper curve is the structure of the rough interface produced by the simulation. The lower curve is the roughness profile of a real stylolite. The figure is taken from Francois Renard et al. [20]

growth of the roughness amplitude follows a power law in time in all three cases, but the two smallest systems have a growth exponent of 0.5 and 0.54 while the biggest system has a growth exponent of 0.8. The two smallest systems are believed to grow in a regime dominated by the surface energy. The biggest system is growing in a regime dominated by elastic energy.

2.6.3 Roughening due to surface instability and noise

Francois Renard et al. [20] have measured the roughness of stylolite surfaces. They have removed the rock on one side of the stylolite surface and measured the roughness using both optical and mechanical profilometers. They found that the surfaces had a self-affine roughness with a crossover length separating the two self-affine regimes. They then made a numerical model with three driving forces; long range elastic interactions, surface tension, and quenched noise. In addition to the battle between the roughening elastic energy and the smoothing surface energy they added noise to the system. The model considers a solid-liquid interface. The model produces an interface with roughness very much like the measured roughness of their samples.

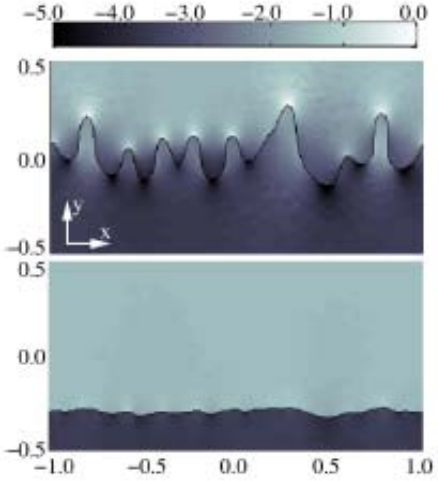

Figure 2.9: The figures show the initial stage (lower panel) and a later stage in the roughening. The figure is taken from Angheluta et al. [6]

2.6.4 Roughening due to instability of solid solid interfaces

L. Angheluta et al. have made a model using linear stability analysis [6]. This model considers a solid-solid interface instead of a solid-liquid interface, which the Asaro-Tiller-Grindfeld instability considers. The system consists of two solid blocks separated by an interface with a random perturbation. The interface represents a jump in elastic properties, otherwise the two solids are identical. The system is stressed normal to the direction of the interface. There is no transport of solute in the model, only a phase change at the interface.

The instability in this model is driven by the jump in elastic properties in the two solids. The stress the system is exposed to is driving a phase change on the boundary. The more elastic solid, which is the upper one, is transformed into the less elastic solid at the interface. This way the interface is moving upward in the system.
This phase change from more to less elastic can be seen as a porosity change of the solid and the elastic jump is caused by a jump in porosity. The density of the two solids are though the same. There is also a version of the model with a jump in density as well, which also leads to an unstable interface. The phase change on the interface can then be seen as a dissolution of material

due to stress concentration and a precipitation of this material in the pore space. This process leads to a movement of the interface between high and low elasticity. When we look at the system this way, we assume that the system is limited by the dissolution. The dissolved material is diffusing out into the pore space where it precipitates.

We have now looked at three different models for roughening of an initial flat surface with or without some perturbation. They all produce rough surfaces that look more or less like the natural stylolites. In two of the models there is random noise introduced. These models produce patterns with a more teeth-like geometry (sharper edges) than the model without noise. This model has a smoother surface with round edges. This indicates that the random noise is important for the shape of the rough surface. The noise seems to have a sharpening effect on the curved parts of the surface. Two of the models use linear stability analysis, one of them considers a solid liquid interface, and one considers a solid solid interface. These three models are different in many ways, but they all produce roughening of an interface. This might indicate that there can be several roughening mechanisms involved in the roughening of stylolites.
One thing that is important for the laboratory experiments is the roughening rates in the different models. In the model made by Koehn et al. the roughening rate follows a power law $W \propto t^{\beta}$ where beta varies from 0.5 to 0.8. Compared with the model created by Anghelute et al. this is very slow. In their model the roughening first grows exponentially $W \propto e^{t}$ and later as $W \propto t^{2}$. It is not surprising that the roughening rate of the solid-solid interface is larger. To move an interface set by a jump in porosity you need to dissolve and/or precipitation an amount of material proportional to the porosity jump. To move a solid-liquid interface the same length you need to dissolve and/or precipitate much more material. This will, off course, take more time.

Chapter 3

Methods and materials

3.1 NaCl

An experiment modelling compaction of chalk-rich sediments, where pressure solution is the main compaction process, require a model material that dissolves quickly in order to operate in a reasonable time-scale. Sodium Chloride dissolves fast and it is a common model material to use in compaction experiments. It has been proven, for instance, that clay enhances the compaction of salt by up to 200 percent [19]. By using common model materials, existing experimental results as this, can give useful knowledge about the process. As model material in a compaction experiment sodium chloride seems like a good choice. The fact that there are no reported observations of stylolites in halite (the mineral form of NaCl) does not mean that it is a bad model material for an experiment in a laboratory environment. The pressures, temperatures and time-scales are totally different in the laboratory than out in nature where rocks are formed, and NaCl is suited the lab environment where we try to simulate a process of compaction of sediments.

3.2 Digital images

In modern cameras, light is caught with a digital CCD chip instead of light sensitive films as in traditional cameras. A CCD chip is a light sensitive chip that is divided into small areas called pixels. The number of pixels can vary from around 100000 (0.1 megapixels) to above 50000000 (50 megapixels) depending on the camera. The number of pixels on the CCD chip limit the resolution of the photos you take. When light hits the CCD chip, each pixel will register the intensity of the light that hits it as an integer value between 0 and 255. A 6 megapixel camera normally has a 3000×2000 pixel CCD

Molecular formula	NaCl
Molar mass	$58,44277 g/mol$
Density	$2,16 g/cm^3$, solid
Melting point	$801°C$
Boiling point	$1465°C$
Solubility in water	$35,9 g/100 ml (25°C)$
Deforms plastically at	$20 MPa (25°C)$

Table 3.1:

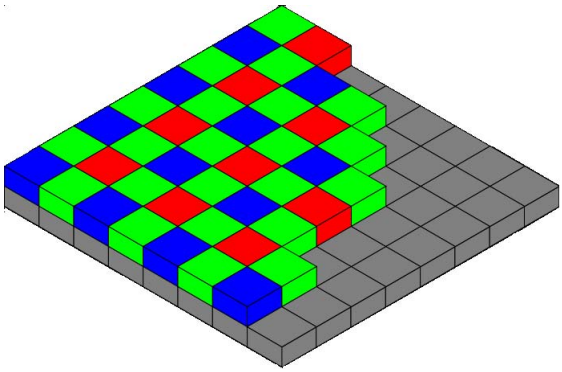

Figure 3.1: A Bayer filter with its red, green and blue areas. The grey layer under the filter is the CCD chip. The figure is taken from [2]

chip, so the photo you take is stored as a 3000×2000 matrix with integers between 0 and 255 representing the light intensity. A camera like this only takes grey scale photos. In a colour camera there is a Bayer filter in front of the CCD chip. This is a light filter that lets through red, green and blue light in different areas. See figure 3.1. Half of the pixels on the CCD are registering green, one fourth are registering red and one fourth blue. Green is overrepresented because the human eye is more sensitive to green light. This way, the actual resolution in each colour is less than the number of pixels on the CCD. The colour image is stored as three 3000×2000 matrices, one for each colour, where they interpolate colour information to create full matrices.

The photos taken of the experiments are just matrices with intensities of the different colours red, green and blue (RGB). So when we are talking about images in the text we are referring to these matrices. In our treatment of the images we do not need the colour information. We will correlate the values in the matrices in different images to find displacement of different regions in

the experiment, this will be explained later, so dealing with all three matrices instead of one will just make the process more time demanding. We therefore convert the colour image into a grey scale image where the information in the three colour matrices are used to make one matrix containing only intensity. One grey scale image is consisting of 6 million intensities distributed in a 3000×2000 matrix like this:

$$I_G = \begin{pmatrix} I_{1,1} & \cdots & I_{1,3000} \\ \vdots & \ddots & \vdots \\ I_{2000,1} & \cdots & I_{2000,3000} \end{pmatrix}$$

where the indices running from 0 to 2000 and 3000 respectively, corresponds to physical coordinates in the lab reference frame. The intensity values in the grey scale image is between 0 and 1.
The images are saved as TIFF files which is a format using lossless compression or no compression. Therefore no information is lost in the saving process.

3.3 Image analysis

All the image analysis is done using MATLAB. The scripts can be found in the appendix.

A series of photos is taken during the compaction of a material and we want to use them to acquire the displacement- and strain fields. One way to do this is to use correlation. When both the camera and the compacting material is fixed, the only movement from one photo to the next is the actual compaction. To find the displacement field of the compaction the first photo is divided into small areas. We then use correlation to recognise these small areas in the next photo and by comparing the coordinates of the areas in the first to those in the second photo we get their displacements. This method is thoroughly explained later in this chapter. We now have a set of displacement fields, one for each time step in the compaction. These can be used to derive strain fields. With these fields we can reveal the localization of compaction if the compaction is not homogeneous.

3.3.1 Correlation

We implement the correlation method described in the article of Hung et al. [13].

We want to map the displacement field of a compacting material using correlation. We have a series of images taken during the experiment and we want to find the relative displacement of the different regions in the experiment between every image. We will use a correlation method using two images at the time, first image number 1 and 2, then image number 2 and 3, etc. We will then end up with one displacement field for every time step (time separating the images is 1 hour). The first thing to do is to choose a resolution for the displacement field. We must choose a step, s, saying that for every s pixels in the image we want to find the relative displacement of the compacting material in the time step between one image (I_1) and the next image (I_2). Choosing s gives us the resolution of the displacement field (represented by the displacement matrix D) and a resolution ratio between the image and the displacement field R_{res}. To find the displacement of the area covered by one pixel we have to choose an area around the pixel that is big enough to contain enough structure to make it unique. This correlation area A_c can vary in size from experiment to experiment, depending on how homogeneous the images are and the resolution of the camera used. For the first position in the displacement matrix ($D_{1,1}$), it is picked out an area of size A_c from I_1, we call this area $I_{1,loc}$. We want to detect the area from I_2 ($I_{2,loc}$) that gives the best correlation with $I_{1,loc}$. The correlation coefficient r_c is the normalized sum of the pixel-wise multiplication of $I_{1,loc}$ and $I_{2,loc}$ (In the expression for r $I_{1,loc}$ and $I_{2,loc}$ are called $I1$ and $I2$ to avoid too many indexes, i and j are the pixel coordinates):

$$r_c = \frac{\sum_{i,j} I1_{i,j} I2_{i,j}}{\sqrt{\sum_{i,j} I1i,jI1i,j}\sqrt{\sum_{i,j} I2_{i,j} I2_{i,j}}}$$

By comparing the coordinates of $I_{1,loc}$ and $I_{2,loc}$, we get the displacement of $I_{1,loc}$ in the time step between I_1 and I_2. This displacement is measured in pixels. The search for the $I_{2,loc}$ that gives the best correlation is a process that demands time and resources.
A good correlation gives a high r_c value, but in the program we calculate $r = 1 - r_c$ instead of just r_c so we are actually looking for the lowest value. To search through the whole image, you must calculate r 6 million times (for a 6 megapixel camera) for every place in the displacement matrix. Therefore it is absolutely necessary to limit the search area. This limits are set to the maximum expected displacements in all directions. x_u is the maximum expected displacement upward. In a compacting system x_u is obviously very small. x_d is the maximum expected displacement in the compaction direction.

It is mainly in this direction it is meaningful to search, so this is the absolutely biggest length. x_l and x_r are the maximum expected displacement in left and right direction. These lengths are also small since we do not expect much horizontal displacement in our compacting system. There is then four lengths limiting the search area.
But we can limit the number of times we have to calculate r even more by using the steepest descent method. This method starts from one given starting point and correlates $I_{1,loc}$ and $I_{2,loc}$ with a search area that goes one pixel out from the starting point in all directions. This gives a 3×3 r matrix. The best correlation value of these 9 is the starting point in the next round. This is repeated until the best correlation is the centre value in the 3×3 matrix. This way we have followed the steepest way to the best correlation. The initial starting point for the steepest descent method is important for the time it will take to find the best correlation. To find the best starting point we do a coarse minimum search in our first search area limited by x_u, x_d, x_l and x_r. We use the best correlation value from this coarse search as a starting point for the steepest descent method. So instead of calculating r for every point in our search area we first do a coarse search and from this search best value follow the steepest way to the best correlation.
We have now found one displacement and need to repeat these methods to complete the displacement matrix and find the complete displacement field of the compacting experiment in the time step between I_1 and I_2. Then the whole process must be repeated for I_2 and I_3 etc. In the end the result is a set of displacement fields, one for each time step in the compaction.

Fitting polynomial

If the displacement of the compacting material in one time step is very small, band structures can form because of the discreteness of the displacement. The correlation method gives the displacement in whole pixels. If you have a system with zero displacement at the bottom and one pixel displacement on the top and the compaction is homogeneous, the displacement field should be linearly increasing from zero at the bottom to one at the top. Instead the displacement is zero in the lower half of the system and one in the upper half. This effect can cause a band structure in low displacement systems. To avoid this effect we can increase the resolution of the displacement to sub pixel. To get sub-pixel resolution on the displacement when correlating two photos a polynomial needs to be fitted to the r matrix that contains the correlation coefficients. When the lowest value in the r matrix is found, the displacement is accurate down to a hole pixel. To get-sub pixel accuracy on the displacement a second order polynomial is fitted to the 3×3 area

on the r matrix where the lowest value is in the middle. The coordinates of the bottom of the fitted polynomial will give sub-pixel accuracy on the displacement. We have now nine correlation values and we are going to use a second order polynomial. This gives an over-determined set of equations; nine equations and six unknowns. The set of equations is:

$$\begin{aligned} r_1 &= ax_1^2 + by_1^2 + cx_1y_1 + dx_1 + ey_1 + f \\ r_2 &= ax_2^2 + by_1^2 + cx_2y_1 + dx_2 + ey_1 + f \\ r_3 &= ax_3^2 + by_1^2 + cx_3y_1 + dx_3 + ey_1 + f \\ r_4 &= ax_1^2 + by_2^2 + cx_1y_2 + dx_1 + ey_2 + f \\ &\vdots \\ r_9 &= ax_3^2 + by_3^2 + cx_3y_3 + dx_3 + ey_3 + f \end{aligned}$$

On matrix form the set we need to solve looks like this:

$$\begin{pmatrix} r_1 \\ r_2 \\ r_3 \\ r_4 \\ \vdots \\ r_9 \end{pmatrix} = \begin{pmatrix} x_1^2 & y_1^2 & x_1y_1 & x_1 & y_1 & 1 \\ x_2^2 & y_1^2 & x_2y_1 & x_2 & y_1 & 1 \\ x_3^2 & y_1^2 & x_3y_1 & x_3 & y_1 & 1 \\ x_1^2 & y_2^2 & x_1y_2 & x_1 & y_2 & 1 \\ \vdots & \vdots & \vdots & \vdots & \vdots & \vdots \\ x_3^2 & y_3^2 & x_3y_3 & x_3 & y_3 & 1 \end{pmatrix} \begin{pmatrix} a \\ b \\ c \\ d \\ e \\ f \end{pmatrix}$$

In an over-determined set of equations like this there is no set of coefficients(a, b, c, d, e and f) that satisfy the sum:

$$\sum_{i,j,k} \left(\left(ax_i^2 + by_j^2 + cx_iy_j + dx_i + ey_j + f \right) - r_k \right) = 0$$

where $i = 1, 2, 3, 1, 2, 3, 1, 2, 3$, $j = 1, 1, 1, 2, 2, 2, 3, 3, 3$ and $k = 1, 2, 3, 4, 5, 6, 7, 8, 9$.

The solution we get is then a set of coefficients that minimizes this sum:

$$\sum_{i,j,k} \left(\left(ax_i^2 + by_j^2 + cx_iy_j + dx_i + ey_j + f \right) - r_k \right)^2$$

.

(same i, j and k as the former sum.)

We now have a surface given by the function: $r = ax^2 + by^2 + cxy + dx + ey + f$ where we now know the coefficients. By derivating this function and finding

the coordinates of the point where $\frac{\partial r}{\partial x} = \frac{\partial r}{\partial y} = 0$ the displacement is found with sub-pixel resolution.

To fit a polynomial to small areas in a matrix is also helpful when deriving the strain from displacement fields. The derivatives of the fitted polynomial are then used instead of neighbouring pixels.

3.3.2 Preparing photos for correlation

Before the correlation our grey scale images are "cleaned". A photo of a granular material like compacting salt has some structures with high contrast and some with low contrast. The correlation method is more sensitive to light changes and other noise when the contrast is low. By removing the low contrast structures from the image before the correlation, the method is more likely to find the best correlation in the correct place and give right displacement. So what we do in this "cleaning" is to smooth out the structures that have small variations in intensity and keep the structures that have large variations. In practice this is to keep the bright and dark spots and remove the background of the image. This is done by calculating the standard deviation of the distribution of pixel values. We calculate the standard deviation in smaller region of the image and clean up these regions individually to avoid trouble because of intensity gradients. The standard deviation is:

$$\sigma = \sqrt{\frac{1}{N}\sum_{i=1}^{N}(x_i - \bar{x})^2}$$

where N is the number of pixels, x_i are the pixel values and $\bar{x}$ is the mean of the pixel values: $\bar{x} = \frac{1}{N}\sum_{i=1}^{N} x_i$. Every pixel with a value in the range $[\bar{x} - \sigma, \bar{x} + \sigma]$ is given the value zero. The pixels with lower values are given the value $x_{new} = x_{old} - (\bar{x} - \sigma)$ and pixels with higher values are given the value $x_{new} = x_{old} - (\bar{x} + \sigma)$. The photo now has positive valued bright and negative valued dark spots on a zero valued background.

3.3.3 Errors in the correlation method

When we are calculating the displacement fields, we have to choose a resolution for these fields. We have to choose how often it is necessary to find the displacement. The area we use in the correlation is often bigger than the

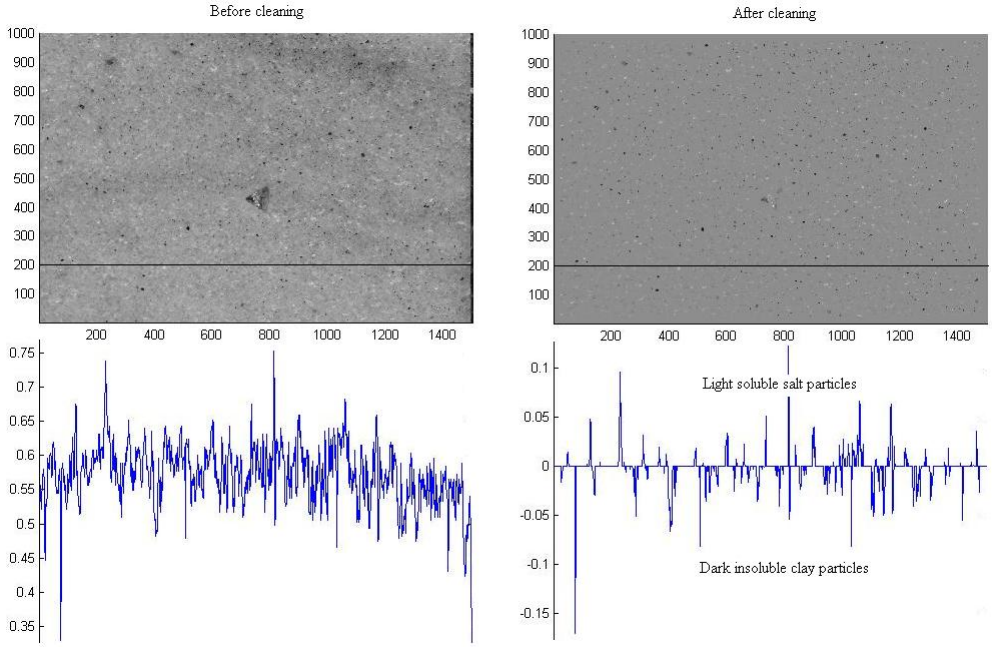

Figure 3.2: Segment of a photo from one of the powder compaction experiments with a hard inclusion before and after it is cleaned.

distance between the points where we measure displacement. This is a consequence of the need to have a correlation area big enough to be unique and that we want high resolution on the displacement field. So the correlation area we use to find the displacement in one point will overlap the correlation area we use in the neighbouring point. The area that is overlapping will off course have the same displacement. If the correlation areas are big the overlapping area will be bigger than the non overlapping part and it will dominate the correlation result and the two neighbouring points in the displacement field will have very similar values. So if there is a slip of some kind inside the cell that causes one grain to move relative to the neighbouring grain, this sharp difference in displacement will get smeared out because of the overlapping correlation areas. This problem is hard to avoid without using correlation areas that are too small. Using a correlation area is, in a way, the same as using a moving average of the displacement. Local jumps or peaks in the displacement will get smeared out. In a compacting system controlled by pressure solution it is not likely to have sudden jumps in displacement and the loss of details will therefore not be that big.
Another possible error is the steepest descent method. If there is a local minimum in the r matrix and the starting point for the steepest descent method is in the vicinity of this minimum we will get the best correlation in the wrong place and get an incorrect displacement for this point. We have plotted the r matrix while running the correlation and have never observed a local minimum but this does not mean that it can never happen.

3.3.4 Strain fields

The displacement matrix we get from the correlation method has two components. One in $x-$ direction (horizontal, normal to compaction direction) and one in $y-$ direction (vertical, compaction direction). So there are actually two matrices which contain the displacement fields in two different directions. We call the displacements in $x-$ direction u and the displacements in $y-$ direction v. We can with these displacements calculate the strain field in the system, which is the most interesting field when studying compaction. The strain tensor is given as:

$$\varepsilon_{ij} = \frac{1}{2}\left(\frac{\partial u_i}{\partial x_j} + \frac{\partial u_j}{\partial x_i}\right)$$

In our two dimensional system with displacement only in two directions the strain tensor looks like this:

$$\varepsilon = \begin{pmatrix} \varepsilon_{xx} & \varepsilon_{xy} \\ \varepsilon_{yx} & \varepsilon_{yy} \end{pmatrix} = \begin{pmatrix} \frac{\partial u}{\partial x} & \frac{1}{2}\left(\frac{\partial u}{\partial y} + \frac{\partial v}{\partial x}\right) \\ \frac{1}{2}\left(\frac{\partial v}{\partial x} + \frac{\partial u}{\partial y}\right) & \frac{\partial v}{\partial y} \end{pmatrix}$$

The most interesting part of the strain is the volumetric strain, which is the trace of the strain tensor.

$$\delta = \frac{\Delta V}{V_0} = \varepsilon_{xx} + \varepsilon_{yy}$$

The volume we are calculating here is off course actually an area since we only have two dimensions. To find the strain fields we use the same method we used to get sub pixel resolution on the displacement fields. We fit a second order polynomial to small areas of the displacement matrices and use the derivatives to calculate the strain. We fit the polynomial $p = ax^2 + by^2 + cxy + dx + ey + f$ to a $n \times n$ big area of each of the two displacement matrices. The smallest possible n is 3 and we have tried for n up to 7, but it doesn't seem to affect the results much. When fitting the polynomial to the small area our coordinate system has the origin in the centre of the small area. Derivating p at the point $x = y = 0$ gives us the following strain: $\varepsilon_{xx} = d_u$, $\varepsilon_{yy} = e_v$ and $\varepsilon_{xy} = \varepsilon_{yx} = \frac{1}{2}(e_u + d_v)$. The indices u and v shows whether the coefficients d and e are from the p fitted to the u matrix with displacements in $x-$ direction or the v matrix with displacements in $y-$ direction.
When this is done for all the values in the displacement field we have a set of complete strain field (ε_{xx}, ε_{yy} and ε_{xy}) of the system in one time step. Doing this for all the displacement fields will give us the full step by step strain evolution.

3.3.5 Sums of displacement and strain fields

Once all the strain fields are acquired, we have to combine them some-how to see the total strain of the system. One way is to add up the strain for all the time steps. The problem with this method is that the system has compacted and therefore changed its shape. One area with given coordinates in one strain field does not represent the same physical area in an area with the same coordinates in another strain field. Because the system has compacted and changed shape, adding the fields together can never give the correct total strain field in more than one region of the system. In our system the most important region is around an inclusion in the compacting material. And we want to add together the strain fields in such a way that the position of the

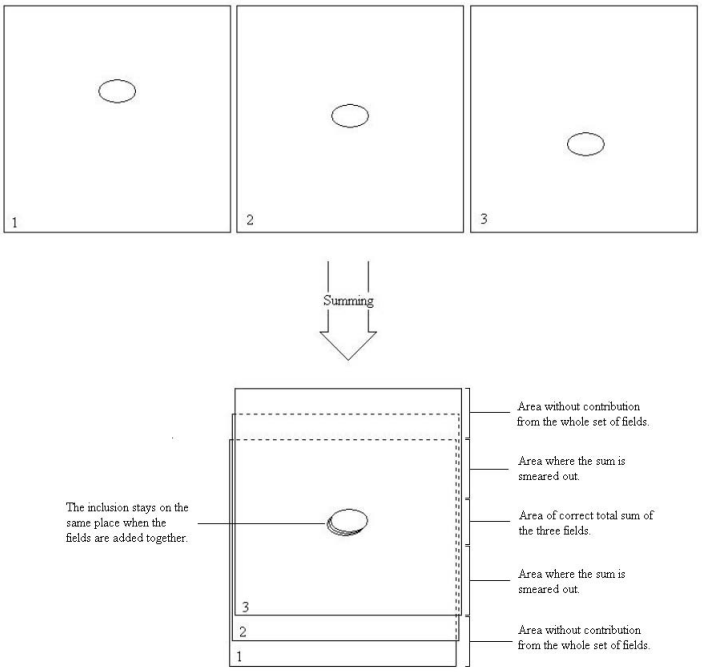

Figure 3.3: The three stress (or displacement) fields 1,2 and 3 are here added together so the inclusion stays stationary and any possible localisation around the inclusion does not get smeared out.

inclusion is constant in the strain fields. This way any localized compaction around the inclusion will not get smeared out as they would do in the outer parts of the field. The smearing effect grows with increasing vertical distance to the inclusion.
We do this summation of both the displacement fields and the strain fields. The method is accurate when looking at areas in the same height as the inclusion but inaccurate for the hole system.

3.3.6 Path lines

In the method described above the field showing the total strain or displacement field is only correct in one part of the system. To get a correct total strain or displacement field we need to consider the compaction and shape change of the system. One way of doing this is to take a set of particles, evenly distributed in the system, and follow them through the compaction. We use the displacement field to follow the particles through the compaction. The particles are represented by a homogeneous grid on top of the first dis-

placement field where the nodes are the particles. The new coordinates for the nodes in the grid going on top of the next displacement field are calculated from the first displacement field. Then the slightly deformed grid is put on top of the second displacement field and we interpolate to find the correct displacement to calculate the next coordinates for the nodes. The grid is deformed and compacted in every time step just as the real system. With this method we can calculate the volumetric strain in the nodes for every time step and get out the total volume reduction of the system with the same accuracy across the entire system.

3.4 Sintering

In one of the experiments we needed sintered blocks of a soluble material. The blocks had to be strong enough to not brake when stressed and they had to be able to lie in saturated fluid without falling apart. We also wanted the salt blocks to have as high porosity as possible. Jean Pierre Gratier and Francois Renard gave us some very strong sintered salt blocks, but they had very low porosity (ca 4 percent). We therefore wanted to make our own sintered samples. The idea was to make a two component sintered block where both components were soluble, and flush out one of the components with with a fluid saturated with the other component. This way we hoped to make a very porous sintered sample. We first tried to make a sintered sample of 100 percent NaCl. The set-up was a glass cylinder with a inner diameter of 15 mm with a brass piston pushing down to apply stress. We filled the glass cylinder with salt powder with grain size of approximately 400 to 700 micron, a dead load of 1,4 kg was put on top of the piston. The sample was then put into an oven which heated the sample from room temperature up to 200 degrees. After 30 minutes at 200 degrees the samples was heated up to 500 degrees where it stayed for 600 minutes before it cooled down slowly. The finished samples was cemented to the walls of the glass cylinders and was hard to get out, but when we got them out they looked nice and strong. When we put them in saturated fluid they almost eminently fell apart. They where not even strong enough to hold their own weight lying in saturated water. The fluid obviously got in to the grain contacts and the samples became useless. It looked difficult to make sintered samples that were strong enough so we decided to use the low porosity samples from Gratier and Renard.

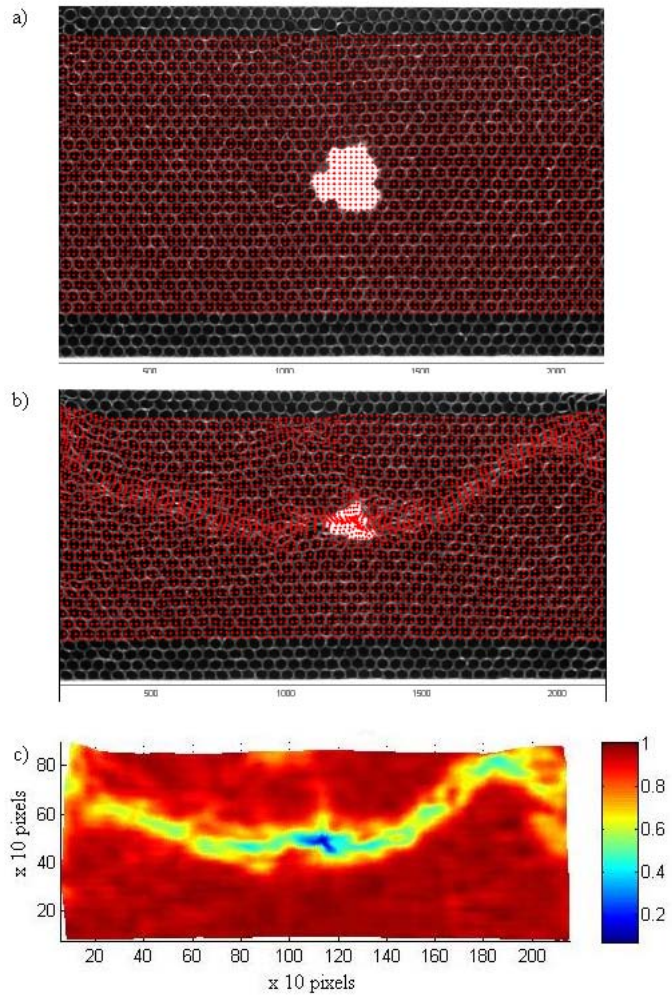

Figure 3.4: a) shows the initial homogeneous distribution of particles on top of the first image in the series. b) shows the deformed grid with particles on top of the last image in the series. The grid has deformed similar to the system in the image. c) shows the final volume we get when we calculate the volumetric strain in all the nodes for all the time steps. Initial volume in all the nodes are 1.

3.5 Roughness measurements with White Light Interferometer

One of the methods that gives highest resolution and accuracy when measuring the structure of a surface is interferometry. There are several different interferometry methods, and one of these is white light interferometry with a Mirau interferometer lens. This method uses a light source that emits white light and a lens that uses a technique with a beam splitter and a reference mirror. The light beam from the light source is split in a beam splitter. A beam splitter is a semitransparent mirror that reflects one part of the light and transmits the rest. The reflected light goes through a microscope objective before it is split by another beam splitter. The transmitted light hits the sample while the reflected light hits a reference surface which is placed on the microscope objective (See lower figure in figure 3.5). The distance from the microscope objective to the beam splitter, D_1, is $f/2$ where f is the focal length of the objective. The white light used in the interferometer consists of a range of wavelenhts. At a given distance from the light source, all the waves in the white light are in phase. The interferometer is calibrated such that the focal point of the objective and the point where all the waves in the white light are in phase, is in the same point. When the distance from the beam splitter to the sample, D_2, is equal to D_1, there will be constructive interference when the light beams are united again above the beam splitter. This constructive interference will appear as a fringe pattern on the images captured by the CCD chip. The images captured by the CCD chip will be analysed and the areas on the sample with a fringe pattern will be detected. These areas are exaterly the distance f from the objective. When the sample is moved vertically the fringes will move around on the sample but always be on the areas that are the distance f from the objective. The sample is moved vertically by piezoelectric motors that are very accurate. By knowing the vertical movement of the sample while monitoring where the fringes are on the sample, the height profile of the sample is obtained.
The interferometers software store the relative heights of the sample as a matrix, and it calculates some surface statistics. The roughness statistics calculated are of interest in this experiment. The measure for roughness we use is

$$R_q = \sqrt{\frac{1}{n}\sum_{i=1}^{n}\left(Z_i - \overline{Z}\right)^2}$$

which is the root mean square of the deviation from the mean height. Z_i is the height in point i and $\overline{Z}$ is the mean height. R_q can be calculated for any

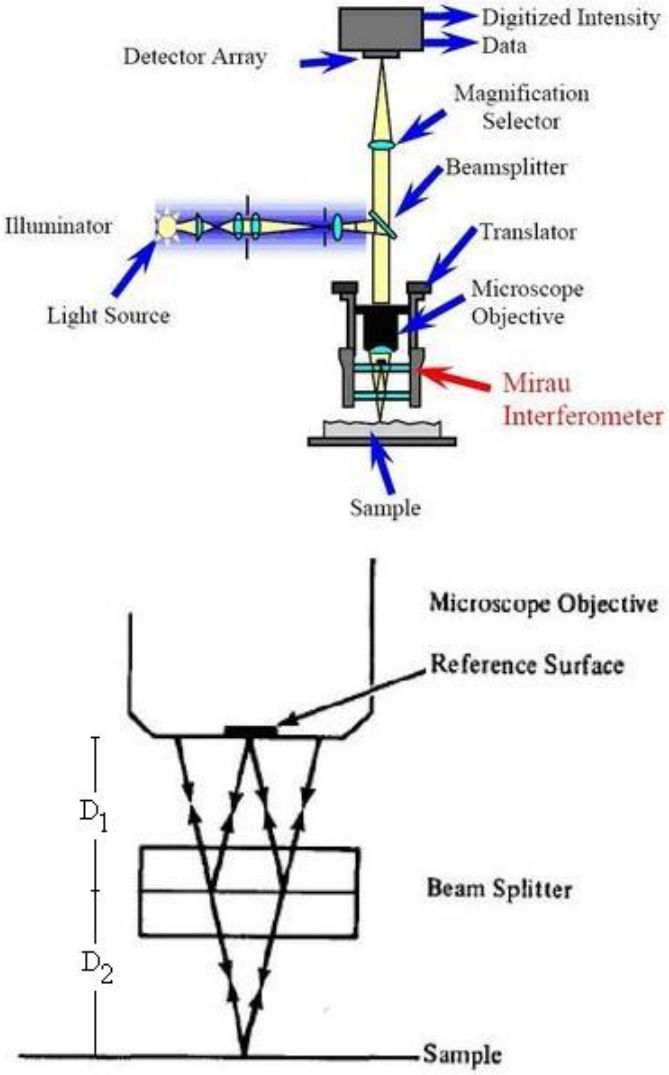

Figure 3.5: The upper figure shows a drawing of a white light interferometer with a Mirau interferometer lens. The lower figure shows a sketch of how the light beams travel through the mirau lens. The figure is taken from [3].

chosen area of the sample.

Chapter 4

Experiments

4.1 Ideas

To answer the questions posed in the introduction we need good experiments. The first question; What happens around an inclusion in a compacting porous material? Will stress concentrations lead to localized compaction and anticrack formation? To answer this, two experiments are made; one with a set-up of compacting elastic drinking straws in a Hele-Shaw cell, and one with a set up of compacting NaCl in a Hele-Shaw cell. The conclusion of the anticrack model and other localization models is that stress concentrations around an inclusion will lead to localized compaction. These stress concentrations are caused by an elastic response from the material compacting. To investigate this we do experiments with two different materials and two different compaction mechanisms. The main compaction mechanism in the NaCl experiment is pressure solution and the compaction mechanism in the drinking straw experiment is mechanical flattening of the drinking straws. These are totally different processes but they are both stress driven and the similarity is that they will both be faster in areas with high stress. The effect of stress concentration should therefore be the same in the two set-ups.
The second question; what happens to a pre-existing flat surface when the system it is in is compacted in the direction normal to the surface direction? To test this we need to compact a system with a flat interface. Polished sintered salt blocks lying on top of each other is compacted in a cylindrical set-up.
The third question; what is the relationship between individual stylolite planes? To try to answer to this question we need to successfully answe the first question.

4.2 Experimental set-up

4.2.1 Powder compaction experiment

In order to test whether the anticrack model is applicable to a system of compacting sediments, we want to do a compacting experiment with pressure solution as the compaction process. The compacting material must be porous and there must be a pre-existing crack or weak spot inside the material. The material has to be soluble. We also want the system to be visible so we can see the development of the experiment. We want to map the strain field in the whole experiment to see if there is homogeneous compaction or if there is some localisation. We want to take photographs of the experiment while it compacts and find the strain field with image analysis.

The first thing we have to do is to choose a model material. We do not want to do it with the chalk rich sediments where you find the stylolites in nature, then our experiment would take thousands of years and we do not have time for that. So we need a model material that is dissolving much faster. Our choice is Sodium Chloride, normal table salt? It dissolves much faster than chalk and it is a common model material. So what kind of set-up do we need to get the measurements we want? Our plan is to monitor the experiment with an optical camera and analyse these photos to map the compaction in the experiment. To be able to take photos of the experiment while compacting it needs to be transparent and two dimensional. A Hele-Shaw cell made out of glass, with a glass piston with a weight on top to apply the stress is a possible set-up. It is transparent, two dimensional and should not be too difficult to make. So how big should the cell be? Pressure solution goes faster the more stress is applied to the salt, but the upper limit is 20 MPa. At 20 MPa salt starts to deform plastically, so the stress must be less than that. This is important when we decide what size we want on the cells. The fact that the cell are made out of glass also put an upper limit to how much weight we can put in the piston. To get high stresses the cells should be small. A possible piston is a microscope plate. A microscope plate is 1 mm thick and 26 mm wide. The area is then 26 mm2. 20 MPa corresponds to a weight of 200 kg per cm2, which again correspond to 50 kg on the piston. The porosity of the salt powder in the cell is between 5 and 50 percent. If we assume the absolute upper limit for the porosity (50 percent), a stress in the grain contacts of 20 MPa correspond to 25 kg on the piston. 25 kg is way too much weight to balance on top of a 1 mm thick glass piston, but we do not want to make a smaller cell because of wall effects and practical reasons like making, sealing and filling the cell. The size of the cells is then chosen to be 1 mm thickness, 26 mm width and the height depend on how much salt we

pour into the cell. We want to do this experiment with both hard and soft inclusions. With a hard inclusion there will be stress concentrations on top and under the inclusion, and with a soft inclusion the stress concentration will be on the sides. To find a hard inclusion is not so difficult. A small glass bead is an excellent inclusion. To find a good soft inclusion is not that easy. A small ball of cotton is one possibility, but it might be difficult to spot it in the photos. Another possible inclusion is an ear plug. It is very visible and soft and should be easy to spot in the photos.

The cell is made totally out of glass. It is made out of two big glass plates that are glued together with 1 mm thick buffers between them. The distance between the buffers are 26 mm. The open space in the cell is then 26 mm wide and 1 mm thick, the exact size of a microscope plate. The bottom and sides of the cell are properly sealed to keep the saturated fluid that is surrounding the salt inside the cell. See figure 4.1 for drawing of the experiment.

We mix clay particles in the salt to enhance the compaction. Renard et al. [19] showed that a 10 percent clay content increase the strain rate of compacting salt aggregates with up to 200 percent, and that the effect of clay where significant already from 1 percent clay content. The clay are also working as passive markers in the image analysis. We pour the salt into the cells and put the inclusions in the middle. we do the experiment with both a glass bead as an inclusion and a ball of ear plug, but not in the same experiment. The only difference is that the anticrack should propagate from the top and/or bottom of the inclusion with a glass bead as inclusion, instead of from the sides which is the case with the soft ear plug ball. It will still propagate normal to the stress direction. The first experiment is with a glass bead. For the following experiments new cells have to be made. The cells can only be used once when the salt will get cemented together and hard to get out of the cell. The first attempt to do the experiment was with a big set up with five cells. We used both soft and hard inclusions. We also varied the grain size. By varying the grain size we for instance vary the number of grain contacts and the volume of each pore. This is parameters that might be important in a set-up where dissolution happens in the grain contacts, precipitation in the pore space, and where diffusion play an important role. In two of the cells we use salt with grain size 106 to 300 microns, in to other cells grain size less than 106 microns. All the cells where mixed with clay. The next two has grain sizes less than 106 microns. The last cell had grain size 106 to 300 microns, and was not mixed with clay and had a soft inclusion. A problem with this set up was that we had to move the camera when taking

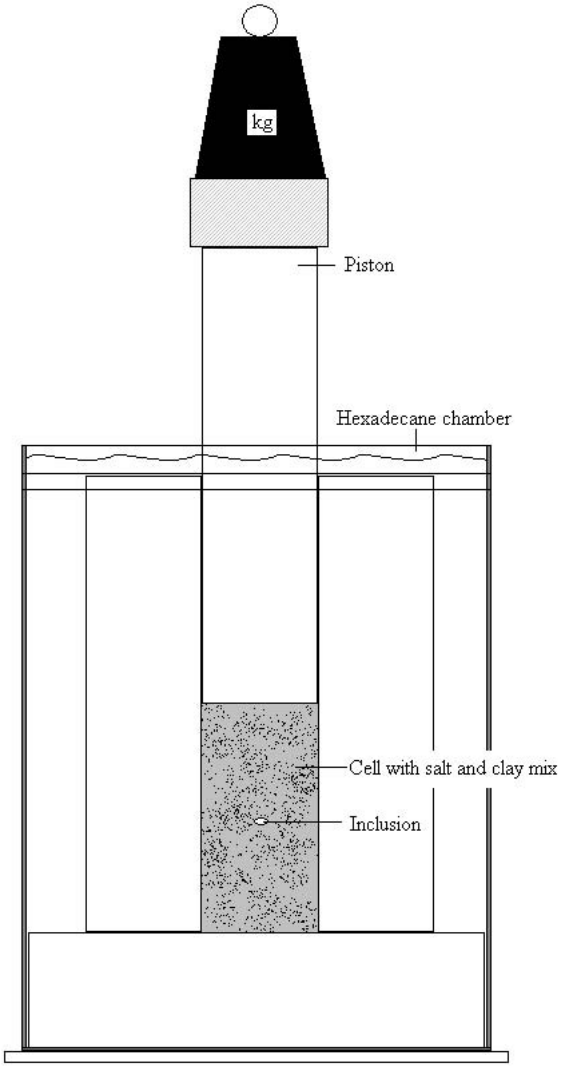

Figure 4.1: Sketch of the Hele-Shaw cell in the powder compaction experiment. Front view of set-up.

photos of the different cells. A consequence of this was that the cell was not in the same place in all the photos. This made the image analysis very difficult. It is possible to correct for this movement, but the compaction rate in these experiments is so small that there is almost no compaction between two pictures. A small error in the correction of the camera movement will then be fatal. The experiments with grain size less than 106 microns where not very successful, and the experiment with no clay compacted slower and the photos where more difficult to analyse. So the final version of the experiment is a set up with only one cell and a fixed camera.

To balance weights on top of a 1mm wide piston is not easy. We had to make something to support the weights. By supporting the piston with a rod that has one end on the piston and the other end on something steady, and then place the weights on the rod over the piston, the set-up will be steady enough. But it is important that the rig that the rod is lying on has the same height as the piston, if not the piston will not get pushed straight down and it will jam in the cell. We then had to make a rig where we easily and with full control could vary the height without moving the rod. We have to decrease the height of the rig as the salt is compacting and the piston is going down. Childhood skills now came handy. We found that the best way to make this rig was with Lego. It is easy, fast and you can build more than steady enough rigs. We then made an adjustable Lego rig that by turning a crank easily goes up or down. Se figure 4.2 to see the Lego rig in the set up.

In the first experiment we used a Nikon D100 camera with a Nikkor 105 mm micro lens. This is a 6 mega pixel camera and with this lens in maximum magnification the field of view (FOV) was ca 26 $\times$ 17 mm. This experiment was with a hard inclusion. The next experiment was also with a hard inclusion, but we now used a different lens. We wanted a higher magnification to do the image analysis easier and to see more clearly what happens close to the inclusion. The lens we used was a Nikon 30 mm lens that we mounted to the camera the wrong way with a special adapter. This way the lens becomes a micro lens with high magnification. The drawback with using the lens this way is that the lens gets extremely dark. The plane where you get a sharp focus is also very limited. But the camera is fixed so there is no problem with a long exposure time and shallow focal plane. In the last of the successful experiments we used a new camera, a D300 with 12 mega pixels. Since the resolution on this camera is twice the resolution on the old D100 we went back to using the Nikkor 105 mm micro lens. The FOV was only 7,2$\times$4,8 mm with the reversed 30 mm lens and that was a bit too small.
The fluid that is surrounding the salt in the cell is water saturated with salt(NaCl). On top of the cell there is a chamber that is 3 mm wide instead

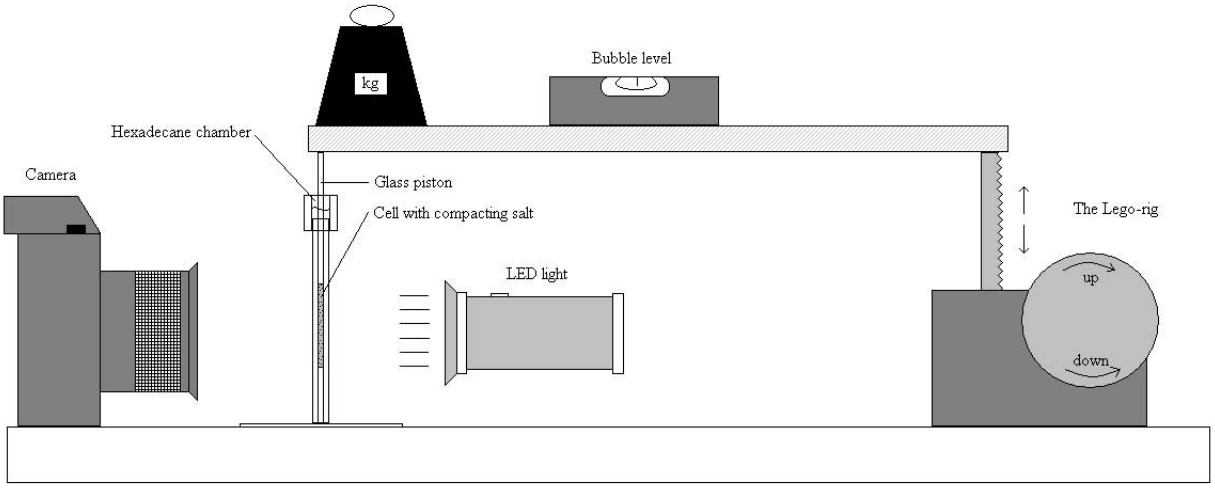

Figure 4.2: Diagram of the powder compaction experiment. Viewed from the side.

of 1 mm like the rest of the cell. This is to prevent capillary rice between the piston and the upper wall of the cell. This chamber is filled with Hexadecane. Hexadecane is an alkane hydrocarbon with the chemical formula $C_{16}H_{34}$. It has a density of 0,77 so it is floating on top of the water. We did not find any evaporation rate but it evaporates very slow. The chamber with hexadecane on top of the saturated water is sealing the cell and preventing the water to evaporate. If the water evaporates there will grow salt crystals on top of the cell and they might jam the piston.
The experiments run for 6 to 8 weeks and the camera is automatically taking a photo every hour. The camera is remote controlled from a computer with Nikon software(Nikon camera control 4 and Nikon camera control pro). Every hour there is a photo of format tiff saved to disc. The dead weight on top of the rod supporting the piston is 1700 grams. The weight is placed as close to the piston as possible, the Lego-rig is not carrying much weight, just supporting the piston.

4.2.2 Drinking straw experiment

The elastic response of the material is essential to get stress concentrations around an inclusion. A requirement for an elastic response is that the grains in the material is some how connected and are not just flowing as individual grains (a fluid). How much freedom the individual grains have to move relative to each other and how this relative movement is affecting the long-range internal stress field is affecting the stress concentration.

The origin for this experiment was that we wanted an experiment that was faster and easier to analyse than the powder compaction experiment. The powder compaction experiment is very time demanding, both to run it and to analyse the results takes time. With an experiment with a different compaction mechanism we could see the effect of an inclusion in a compacting material faster. The first idea for a model material was hollow glass cylinders. This set-up would give a rapid volume reduction in stress concentrations. In the literature we found that Poirier et al. [18] have done compaction experiments with drinking straws. The drinking straws will deform and turn flat in the areas with stress concentration and it is easier to control the speed of the propagation than with breaking glass cylinders. The soft inclusion can be a piece of cotton. The straws will be easy to detect in an image analysis process. The set up can be very similar to the powder compaction experiment only much bigger. A big Hele-Shaw cell with a piston driven by an electronic motor. Since this is a dry experiment we can have the front of the cell open. The big Hele-Shaw cell is built out of plywood with slippery sheeting. This will hopefully give relatively little friction. The piston is made out of the same material. We then attach the cell to a translation rig and the piston to the translation unit on this rig. The translation unit is attached to a thread bar, and to this thread bar we attach an electric motor. The next step is to cut drinking straws into 3 cm long pieces. There is room for approximately 1600 straws in the cell, so it takes some time to cut all the straws.
The drinking straws are then packed in the cell. When all the straws have the same diameter the packing will be close to a close-packed triangular lattice. There will be some frustrations in the packing because wall effects and the inclusion. If the straws have different sizes, the packing will be more disordered. The straws will have more freedom to move relative to each other in this packing than in the close-packed triangular lattice. In the middle of the cell we place a big piece of cotton. We orient the rig almost vertically and place light and camera, see figure 4.3. The speed of the electric motor is controlled by a computer. The speed of the piston is set to between 1 and 2 mm per minute. The camera is controlled by the computer, Nikon Capture 4, and takes a photo every 35 seconds. We had to do the experiment this

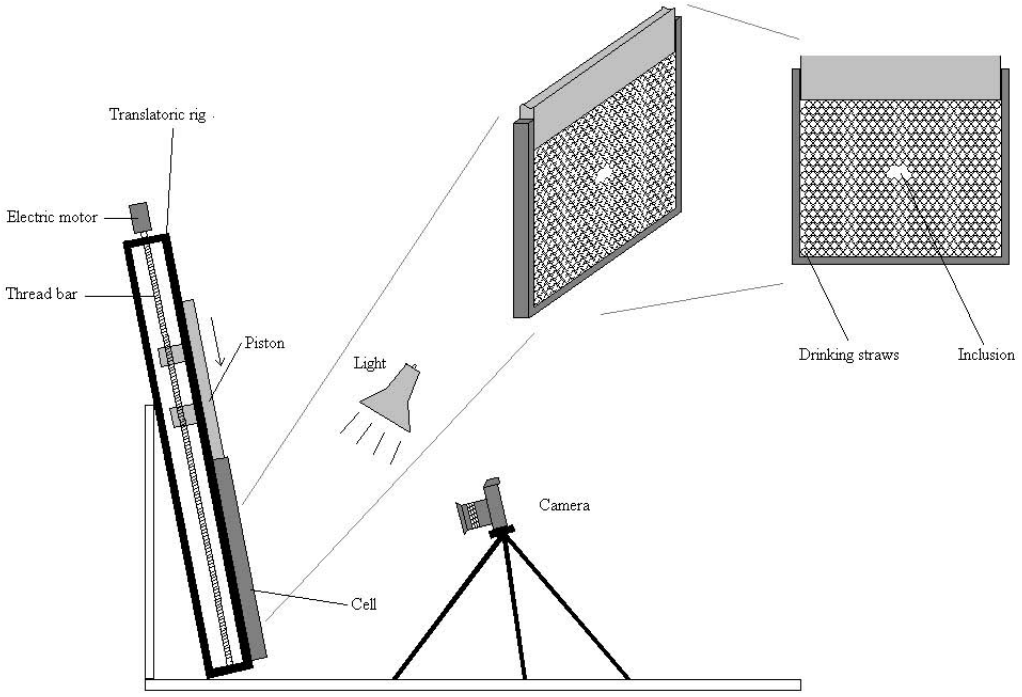

Figure 4.3: Diagram of the drinking straw experiment.

slowly because it took almost 30 seconds to transfer a photo from the camera to the computer.

The photos taken during the experiment will be used to map the strain field in every time step.

4.2.3 Roughening experiment

Another central question in the stylolite study is what happens to a pre-existing flat surface? Say one has a process that gives a flat surface during compaction, for instance an anticrack, will this surface roughen when compacted further? Or does the anticrack have to grow rough to be a suggestion for stylolite formation? A flat anticrack surface would be the perfect starting point for this experiment. This will obviously cause trouble to make so the flat interface between two flat solid samples is the pre-existing surface we are looking at. For this experiment, we chose a cylindrical set-up. The idea is to stack sintered salt samples on top of each other and apply normal

stress with a dead load. This is a three dimensional set-up so we can not monitor the experiment while it is running, like with the two dimensional powder compaction experiment. We can only measure the roughness before and after the experiment. These measurements are done with a white light interferometer (WLI), which is described in chapter 3. It is important to let the experiment run for a sufficiently long period of time. If we abort the experiment too soon we have to start all over again. In this type of experiment where pressure solution is the compacting mechanism and the porosity is very low, the experiment needs a long time to develop. Pressure solution is a very slow process and when the porosity is so low the compaction goes even slower. Thus the experiment will run for 1-2 months.

The set-up of this experiment is made out of glass cylinders with an inner diameter of 15 mm. The cylinder is sealed at the bottom part with a gasket. In the top part of the cylinder a smaller glass cylinder is used as a piston to apply a normal stress to the sintered salt samples that are stacked on top of each other in the cylinder. The cylinder is filled with saturated fluid and a layer of Hexadecane is lying on top to prevent evaporation, just as in the powder compaction experiment. The piston is hollow so fluid can flow through it. This way there is no fluid pressure in the cylinder. The piston is only applying stress in the direction normal to the flat surfaces.

4.2.4 Friction

In all the experiments friction will play a role. In both the drinking straw experiment and powder compaction experiment where we use Hele-Shaw cells, there will be wall friction giving higher stress in the upper parts of the cells. In the drinking straw experiment the friction against the side walls are more important than the back wall. The side walls will cause stress concentrations in the top corners of the cell. In the powder compaction experiment there will be friction against all four walls. This will lead to higher stress in the upper parts of the cell, and the effect will be highest at the sides where there is friction from both side and back/front walls. Since the compaction process in the powder compaction experiment is pressure solution, the compaction rate will be low. The salt will move downward very slowly and there will be a fluid film between the salt and the glass walls. The slow movement and the presence of fluid will reduce the effect of the friction.

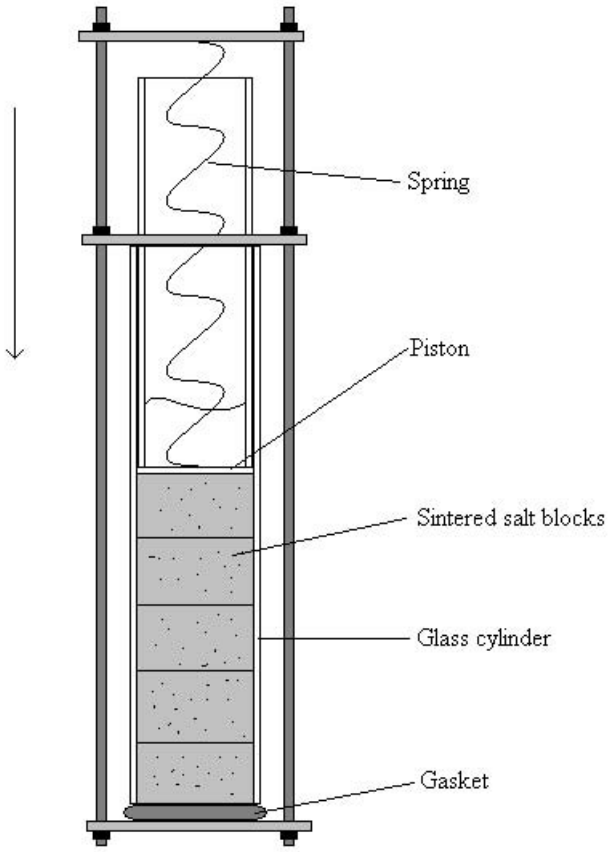

Figure 4.4: Diagram of the roughening experiment.

4.2.5 Attempts to change porosity

Our attempt to sinter our own salt block failed so we decided to use the low porosity blocks from Gratier and Renard in the roughening experiment. The model made by Angheluta et al. [6] have a jump in elastic properties as driving force for the roughening. This jump in elastic properties can be simulated by a jump in porosity. We therefore wanted to do a roughening experiment with blocks with different porosity. We wanted to make the low porous salt blocks more porous. The blocks have very low porosity and it is therefore close to impossible to have any fluid ?owing through them. They are consisting of mostly NaCl which have a solubility that do not dependent much on temperature. This made the task very difficult and we failed to make the blocks more porous.

Chapter 5

Results

5.1 Powder compaction experiment

The goal of these experiments was to see if there is any localization of compaction due to stress concentrations around an inclusion in a set-up where salt grains simulate compacting sediments and pressure solution is the main compacting mechanism. The results from these experiments are acquired using the image analysis methods explained in chapter 3. With the results from this analysis we should be able to unveil if there is any localization of compaction.

5.1.1 Hard inclusion 1

This is the first of the successful powder compaction experiments. We used a hard inclusion and a 105 mm lens for the camera. With this lens we captured the whole width of the cell (26 mm) in the photos. The experiment was compacting for 10 days and compacted 16,5 percent. The front (same side as the camera) of the set-up was illuminated with bright photo lamps in this experiment.

From the correlation method we get out the displacement field in every time step of the compaction, but pressure solution is a very slow process and the compaction goes slowly and it is not likely to see large variations in displacement in one time step. We then sum up all the displacement fields to get the total displacement. It is around the inclusion we expect things to happen so we add together the fields as explained in chapter 3.

Figure 5.1: (Hard inclusion and low magnification).Three of the images taken during the compaction. Images taken in t=0, t=100 hours and t=234 hours.

When we look at the cross sections in the lower figure in figure (5.2) we see a decrease in displacement as we move downward that looks close to linear.

To start out with a homogeneous grid of particles and follow them through the compaction using the displacement field from the correlation can be a very effective way of gather information about the compacting system. When the compaction is completed the particles have moved and by looking at the spacing between the particles we can see how the compaction is distributed. We also use the strain fields to calculate the volume reduction in the small areas we are tracing. When we look at the grid in figure 5.3 we can clearly see that it has followed the compacting material. We can clearly see that the spacing between the particles are smaller after the compaction, and we can see that the concentration of particles are higher in some areas. It is not a big difference but we can see that the compaction is not 100 percent homogeneous.

The path line method is also a good method when looking at volume reduction. By calculating the compressive strain in the areas around the particles we follow we get out the volumetric strain (volume reduction). When we do this for every time step we end up with the final volume change. In figure 5.4 we see the final volume of the small areas. The blue areas has compacted more than the red areas. We see a band structure that has formed normal to the compaction direction. We know there are some errors done when using a correlation area of a considerable size, so we vary the size of the correlation area in the correlation method and do the correlation again. We can see the same band structure when we double the correlation area. The test with half the size of the correlation area clearly shows that this was not big enough

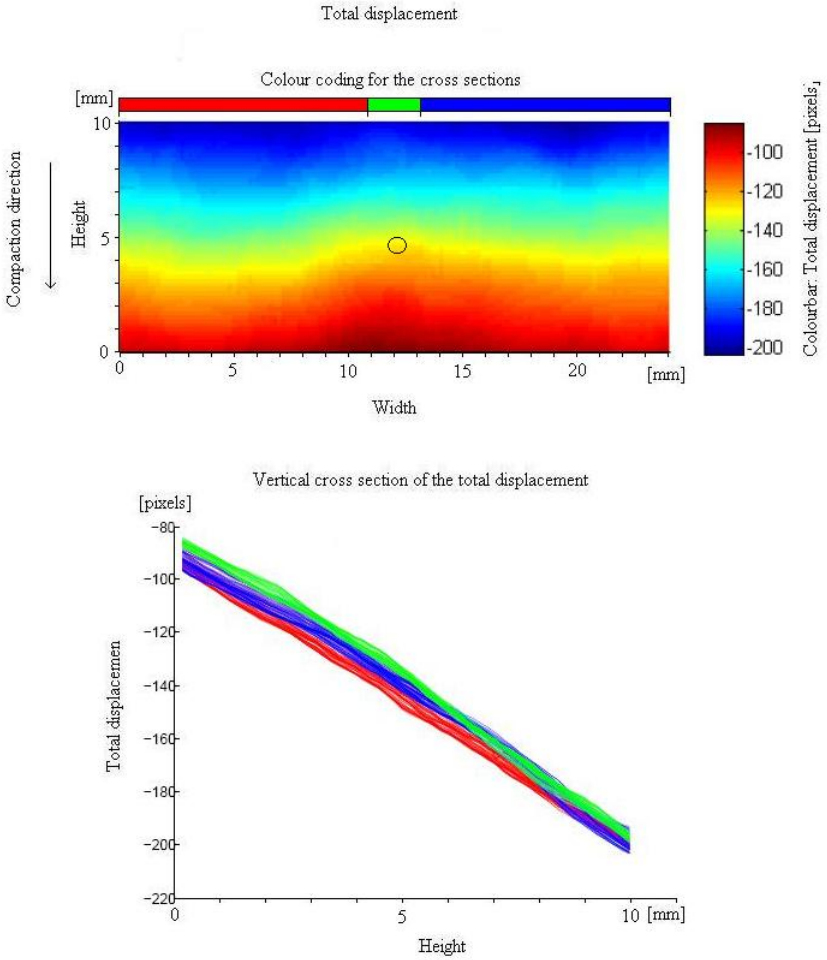

Figure 5.2: (Hard inclusion and low magnification). The upper figure shows the total displacement of the experiment. Under is a plot of vertical cross sections of the total displacement field. The x axis shows height. The y axis shows the total displacement. A high negative number means much displacement because of defined positive direction upward. The colour coding is where in the cell the cross section is from; the red lines are from the left, the blue lines are from the right and the green lines are from the area close to the inclusion.

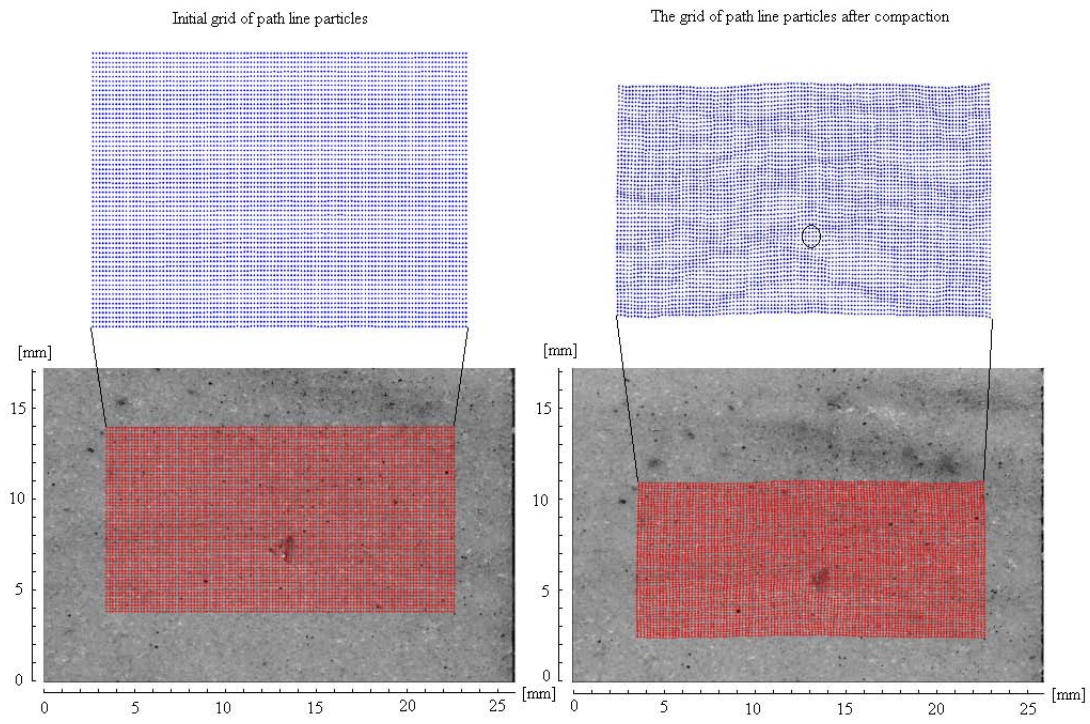

Figure 5.3: (Hard inclusion and low magnification). Path line particles following the compaction.

to give a correct result. In the upper pane in figure 5.4 we see some red areas with a strange shape. The value of these areas are non-physically high (thousands). Even though the correlation area was to small in this case we see a trend showing the same band structure in this case to. We therefore believe the band structure we see is real and not a error from the correlation method.
The band structure of localised compaction do not seem to be linked to the inclusion. The inclusion do not seem to affect the compaction. It looks like there is other mechanisms controlling the localization.

When we look at cross sections normal to the band structure we see a more or less constant spacing between them. The wavelengths of the wavy cross sections are in the range 1,36 mm to 2,14 mm, and the average wavelength is 1,75 mm. See figure 5.5 for the cross sections and their time evolution. The final volume of the different areas in the experiment varies from 0,92 (92 percent of the initial volume, 8 percent compaction) to 0,73 (73 percent of the initial volume, 27 percent compaction). The average total compaction of the system was 16,5 percent. In the band structure the compaction vary between 8 and 27 percent.

The three cross section in figure 5.5 shows some of the wavelengths, but to get a more general measure of the spacing between the bands we use a autocorrelation method. We take the final volume matrix and correlate it with it self. When we do this the correlation coefficient is obviously 1. We then shift all the values in the matrix one pixel up in the vertical direction and correlate this matrix with the matrix without a shift. This gives a lower correlation coefficient. We then shift the matrix two pixels etc. When we plot correlation against number of pixels we shifted the matrix we get a plot with a minimum at the number of pixels shifted corresponding to half a wavelength of the band structure. The areas with high compaction will then be correlated with areas with low compaction in the other matrix and this will give a minimum in the correlation coefficient. Se figure 5.6 for correlation vs shift plot. The shift is calculated from pixels in to mm. This plot shows a minimum in a shift of 1,10 mm which give us a wavelength of 2,20 mm. The dominating spacing in the band structure in this experiment is 2,20 mm. We do the autocorrelation in two directions making a surface of correlation. See figure 5.8

The effect the correlation area size used to find the displacement have on the wavelength is also found using this method. The dominating spacing in the band structure was 13 percent higher when we doubled the correlation area size.

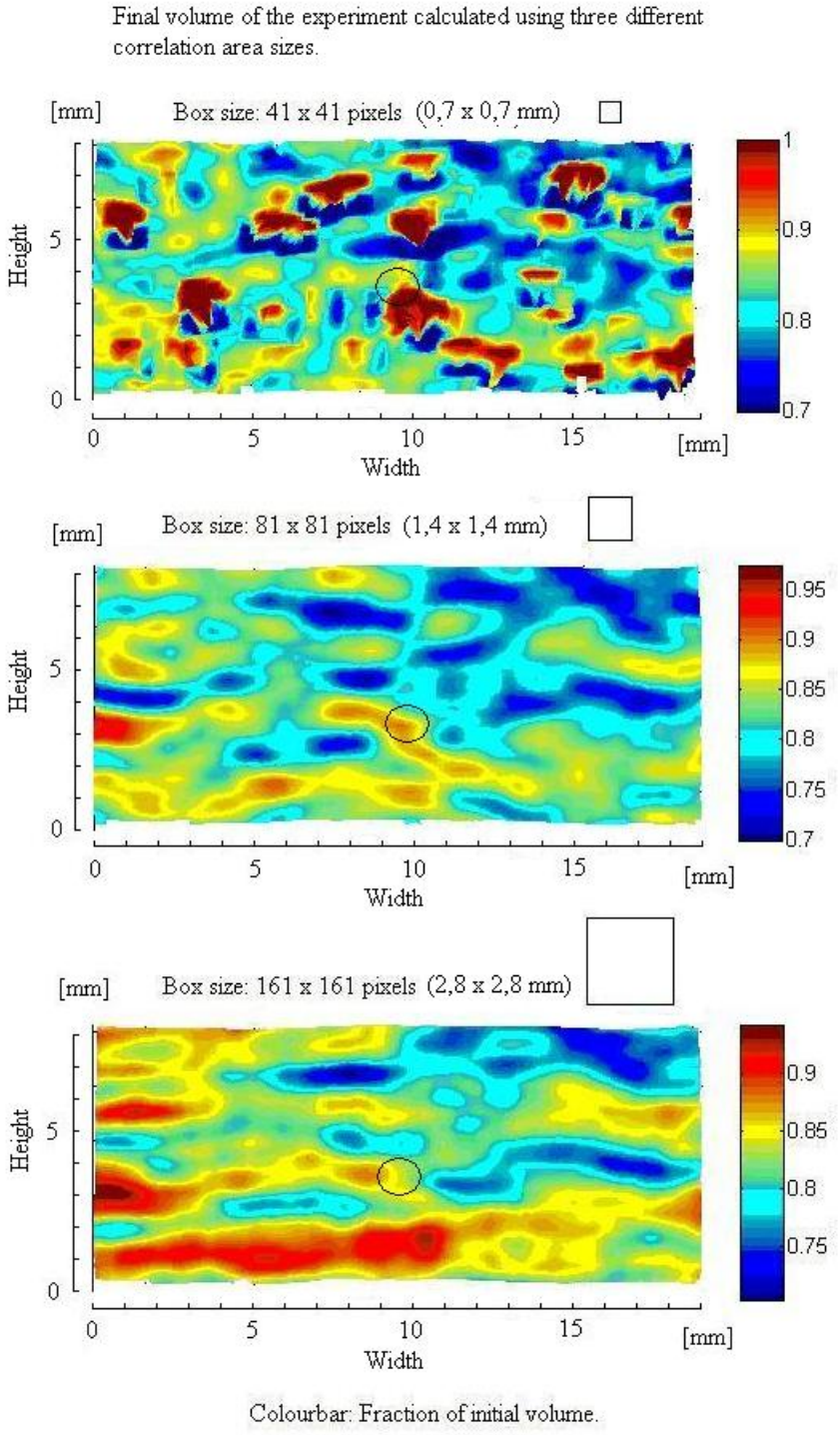

Figure 5.4: (Hard inclusion and low magnification). The plot shows the fraction of the initial volume for correlation done with three different correlation area sizes. The inclusion is drawn as a black circle on each plot.

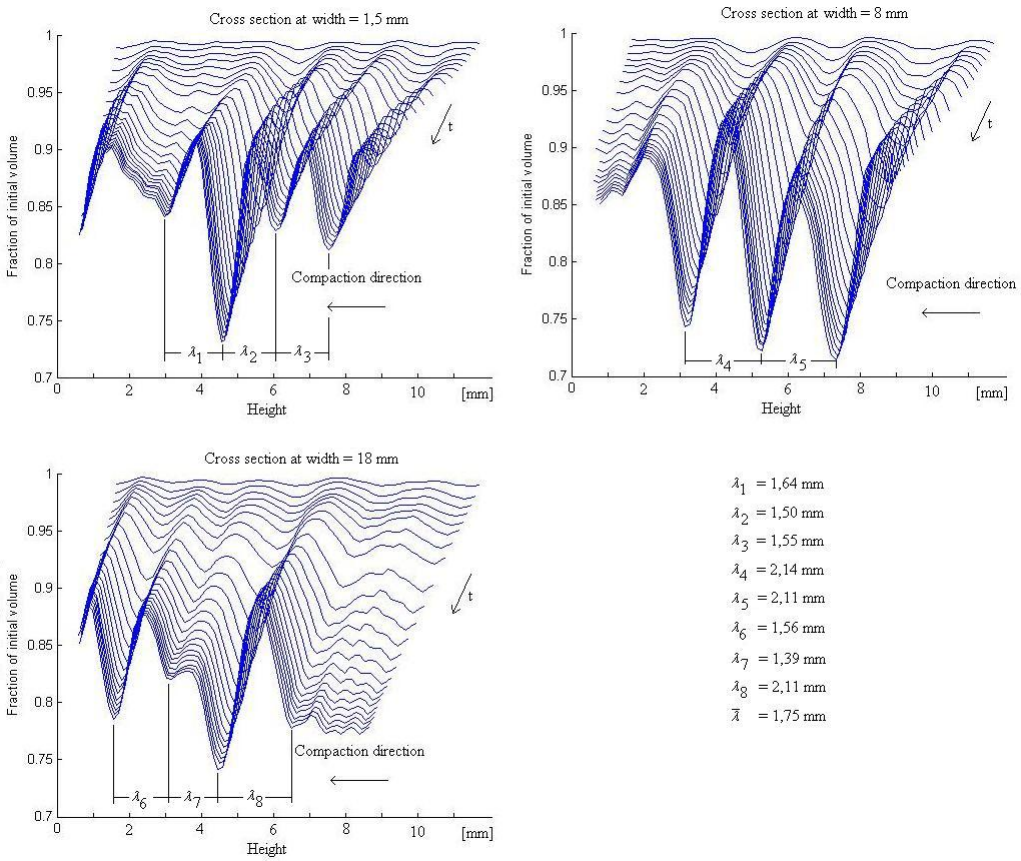

Figure 5.5: (Hard inclusion and low magnification). Vertical cross sections of the "fraction of initial volume field" (middle panel in figure 5.4). The figure shows the time evolution of the volume variations, and wavelengths of the volume variations in the final stage of the compaction.

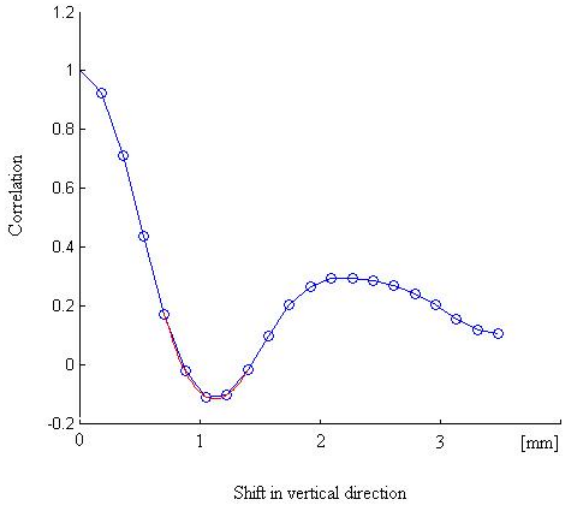

Figure 5.6: Vertical autocorrelation of the final volume matrix. The first minimum gives half the wavelength of the band structure (half the spacing).

We calculated the dominating spacing in all the time steps and got the time evolution of the spacing. We see that it is decreasing along with the compaction of the system.

We see from figure 5.10 and 5.11 that the difference in compaction between the highly compacted areas and the less compacted areas is increasing through the whole compaction. What we observe in this experiment is that the difference is increasing slightly the first 60 hours, it then accelerates and the difference is growing rapidly. It is difficult to say why it has this behaver, it might be clay effects.

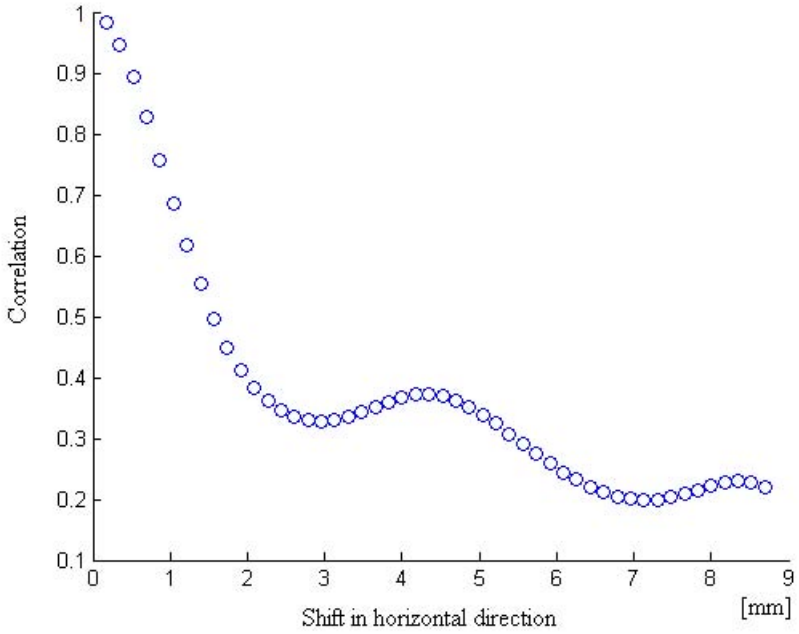

Figure 5.7: Horizontal autocorrelation of the final volume matrix. We see a minimum but the wavelength are much longer than for the autocorrelation in the vertical direction. This means that there is a band structure in the horizontal direction.

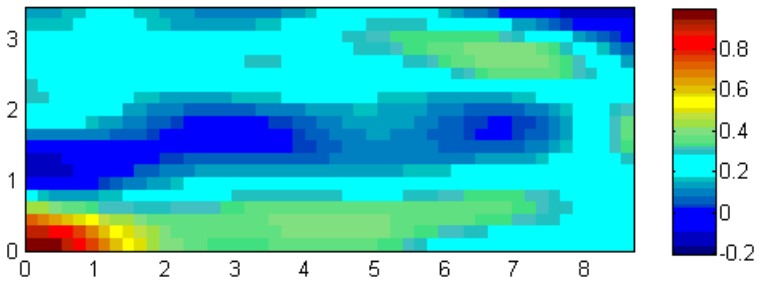

Figure 5.8: The correlation plane from the autocorrelation.

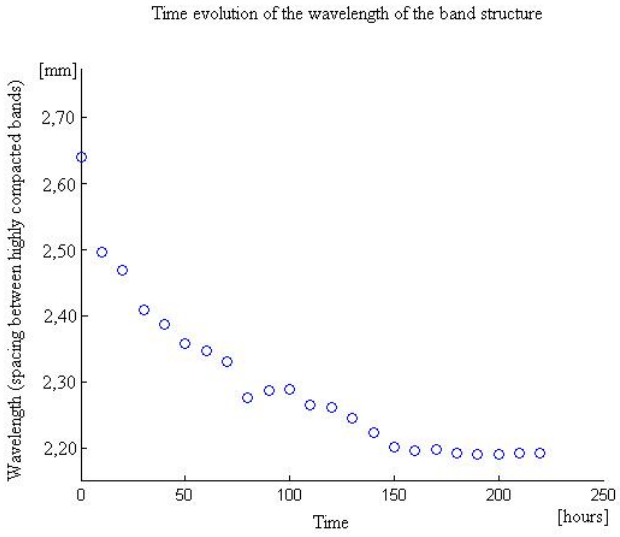

Figure 5.9: The time evolution of the spacing between bands in the structure. The spacings are calculated using the autocorrelation.

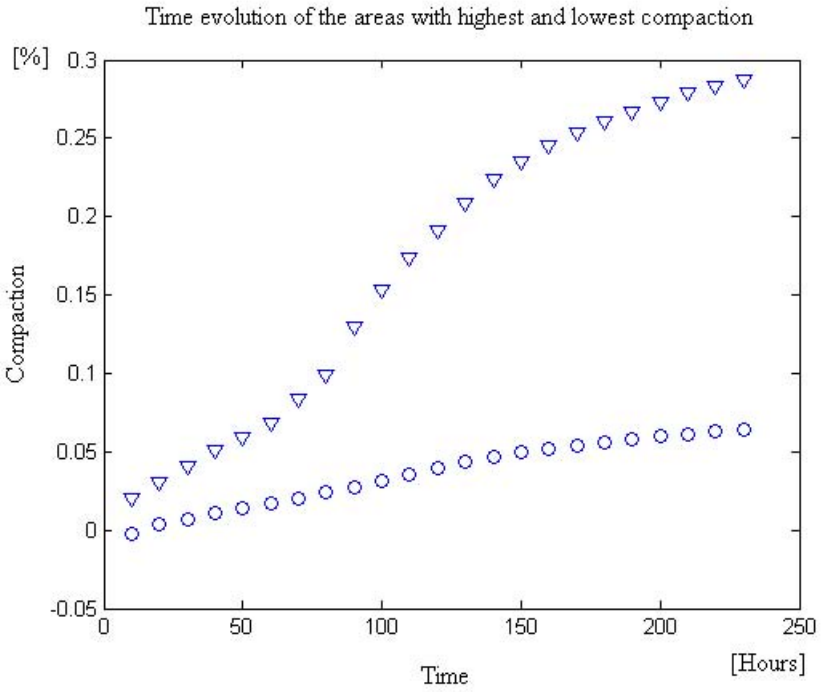

Figure 5.10: The plot shows the time evolution of the compaction in the areas with highest compaction and the areas with lowest compaction. We use the 1 percent with highest and the 1 percent with the lowest compaction values.

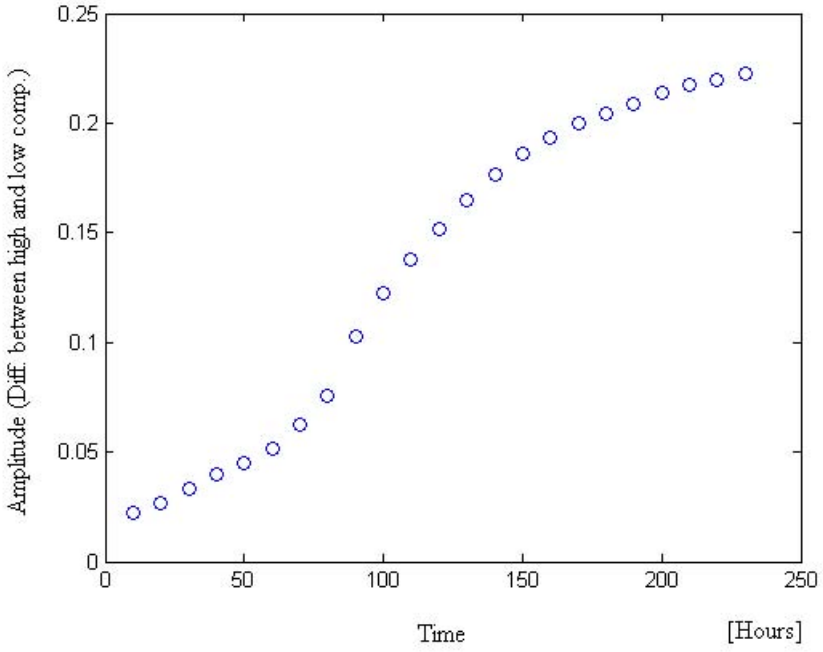

Figure 5.11: The plot shows the difference in compaction value between the highest and lowest compacted areas.

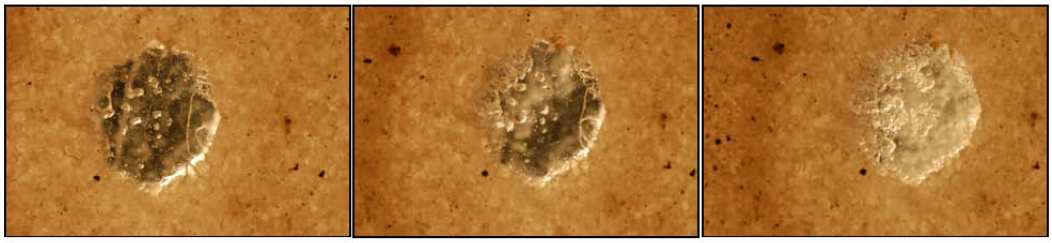

Figure 5.12: (Hard inclusion and high magnification). Three of the images taken during the compaction. Images taken in t=0, t=22 hours and t=269 hours. The compaction direction is from left to right.

5.1.2 Hard inclusion 2

This is the second powder compaction experiments. Also this time we used a hard inclusion, but the field of view was now only $7,2 \times 4,8$ mm since we used the reversed 30 mm lens. The magnification is so high that the inclusion is covering over half the photo width. The inclusion has a diameter of 3 mm. The light set-up is now moved to the back of the cell and light is now shining through the salt.

In this experiment we wanted to look closer at what happens on a smaller scale around the inclusion. There might be a localisation of compaction on a very small scale that was not detectable with the magnification we used on the first experiment. The analysis is done the same way as for the previous experiment, by first using correlation to find the displacement fields, and then using these fields to find total displacement, strain, path lines and volume reduction.

The displacement fields from this experiment had a lot of noise close to and on the inclusion. The reason for this was crystallization of salt on the inclusion. This made the correlation difficult since there was big differences in how things looked from hour to hour. But we could map the displacement on both sides of the inclusion. We can clearly see from the total displacement field (see figure 5.13) that the crystallization of salt has caused trouble. The area covered by the inclusion cannot have variations in the total displacement when the inclusion is hard. So the colour variations showing variations in displacement inside the black circle are non-physical and has to be errors because of the crystallization. It is even more clear when looking at the cross sections. The green lines that are the cross sections covering the area with

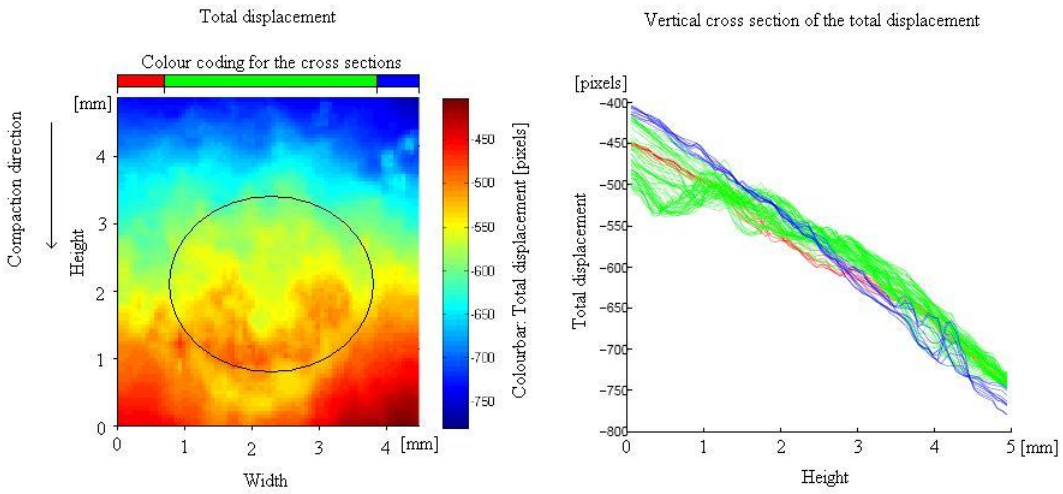

Figure 5.13: (Hard inclusion and high magnification). To the left is the total displacement field of the experiment. The black circle is the inclusion. To the right is a plot of vertical cross sections of the total displacement field. The x axis shows height. The y axis shows the displacement, a high negative number means much displacement because of defined positive direction upward. The cross sections are taken from three different area of the total displacement field. The horizontal colour bar on top of the total displacement field shows the different areas.

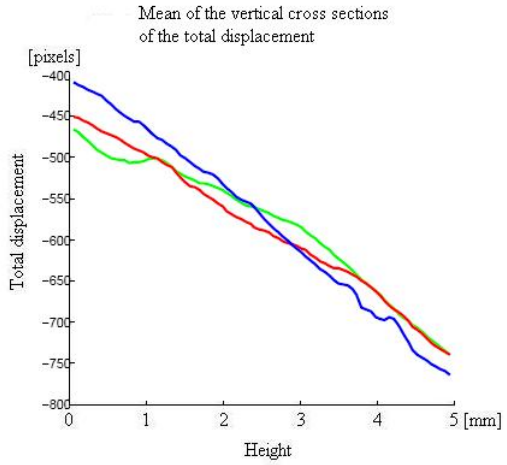

Figure 5.14: (Hard inclusion and high magnification). The figure shows the average of each colour of the cross sections in the left plot in figure 5.13.

the inclusion should be horizontal at the heights covered by the inclusion. The red and blue lines are cross sections from the left and right side of the inclusion. It looks like there is a linear decrease in the displacement as we move downward in the cell. It is easier to look at the average of the lines in figure 5.14. Both the red and the blue line in this plot looks linear. The blue line has a bigger slope than the red one meaning that there is more compaction on the right side of the inclusion than the left.

On the path line plots (figure 5.15 we can clearly see deformation of the grid of particles in the area covered by the inclusion. The inclusion is covering much of the width of the path line particle grid but there is an area of interest on the right side of the inclusion. We see some density variations in the particle grid.

On the final volume field (upper figure in figure 5.16) the noise is dominating the area covered by the inclusion. The inclusion is covering almost the whole width but there is a small area to the right where we can map the evolution of the compaction. See lower figure in figure 5.16 for a cross section of the final volume plot on the right side of the inclusion. This plot also shows the time evolution of the compaction (final volume) in this cross section. Here, as in the "hard inclusion 1" experiment, we get a distribution of wavelengths. See table 5.1 for the different wavelengths. The wavelengths

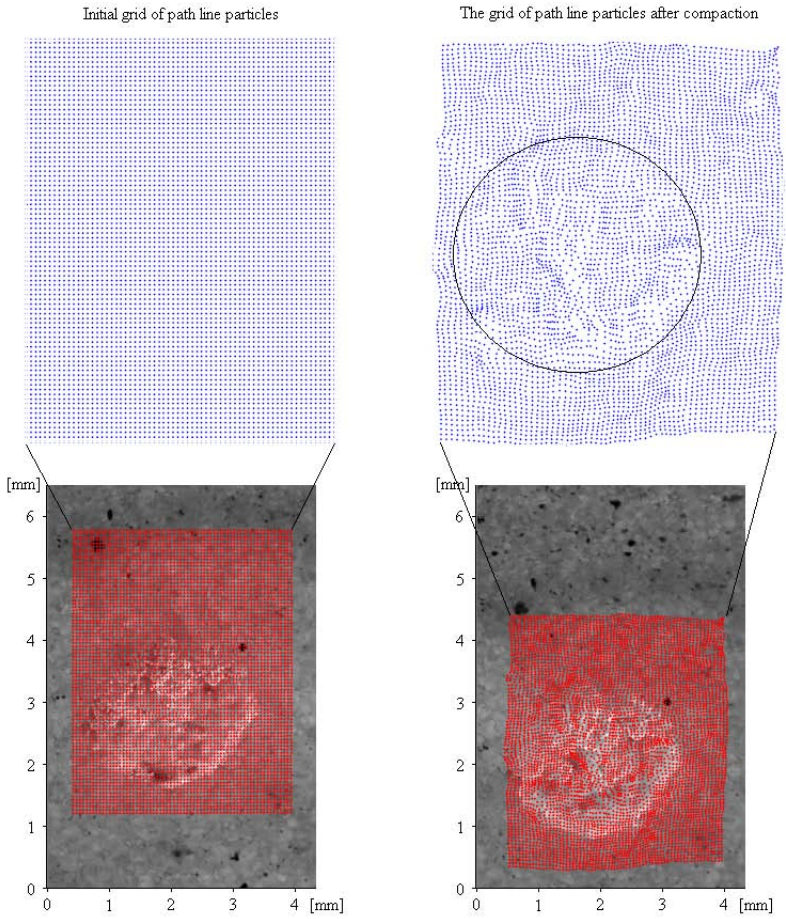

Figure 5.15: (Hard inclusion and high magnification). Path lines following the particles through the compaction.

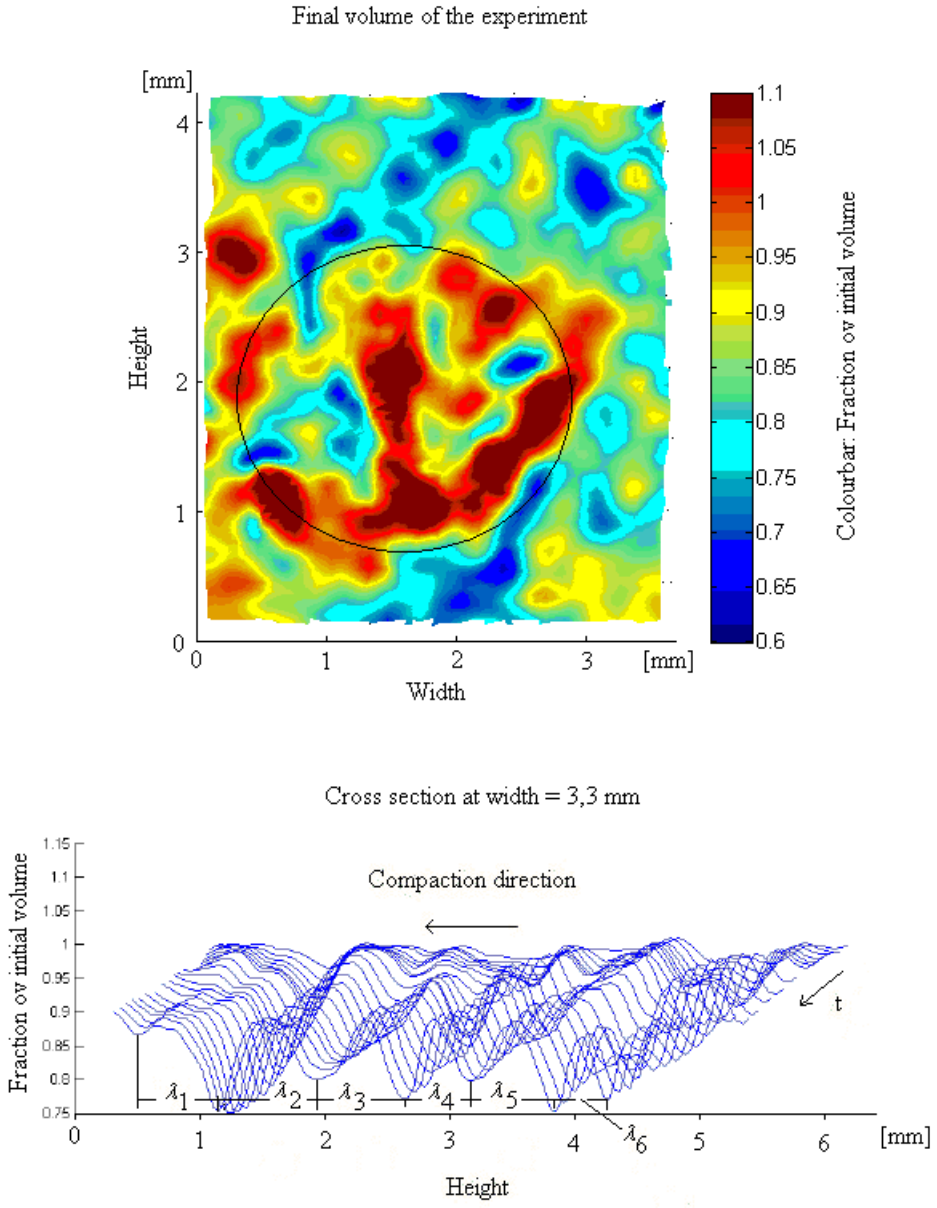

Figure 5.16: (Hard inclusion and high magnification) Final volume field found by calculating the volumetric strain in the path line grid nodes for every time step. The lower figure show the evolution of the volume variations along one vertical cross section at width = 3,3 mm.

wavelength nr. λ_{nr}	length [mm]
λ_1	0,65
λ_2	0,81
λ_3	0,72
λ_4	0,54
λ_5	0,68
λ_6	0,44
$\overline{\lambda}$ (mean)	0,64

Table 5.1: The table is showing the wavelengths in hard inclusion 2.

are in the range 0,44 mm to 0,81 mm and the mean wavelength is 0,64 mm. In "hard inclusion 1" there was a distinct band structure lying in the direction normal to the compaction. In this experiment ("hard inclusion 2") the areas of higher compaction looks more circular. It is though impossible to get a large enough overview of the cell to say if there is a band structure present or not with such a small field of view, but the small area we see indicates no band structure. The final volume of the different areas in the experiment varies from 0,89 (89 percent of the initial volume) to 0,75 (75 percent of the initial volume).

Figure 5.17: Three images from the soft inclusion experiment. The images are taken in t=0, t=30 hours and t=660 hours.

5.1.3 Soft inclusion

In this experiment we used a soft inclusion. We replaced the glass bead with a small piece of a ear-plug. We use the same 105 mm lens as in "hard inclusion 1" but the D100 camera is replaced with a new D300 camera. This increase the quality of the images considerably. The light we used in the two other experiments are replaced with a rig with six LED lamps. This gives a whiter light and the LEDs are not radiating as much heat. The experiment was compacting for 27 days and compacted 21,5 percent.

From the total displacement field (figure 5.18) we can see the effect of the shortening of the soft inclusion in the compaction direction. We can also see this effect as a steeper slope in the part of the green cross section that goes over the inclusion (figure 5.18). In the cross sections on each side of the inclusion we do not see any big variations in the slope that indicates localised compaction.

The deformations of the path line particle grid in figure 5.19 shows a clear vertical shortening of the inclusion. There are also other areas where the particle concentration in the grid are higher. This is easier to see in the plot showing final volume of the system (figure 5.20). In "hard inclusion 1" we see a clear band structure while in this experiment the band structure is more vague. The bands are not as clear but we can see a structure of areas with higher compaction elongated in the direction normal to the compaction direction. An interesting result is that the inclusion do not seem to affect the compaction of the system at all. We can clearly see that the inclusion itself has compacted but this do not seem to affect the rest of the system.

Cross sections of the final volume plot (figure 5.21) shows wavelengths that are shorter than in "hard inclusion 1". We find the dominating spacing of the bands using the correlation method explained earlier in this chapter.

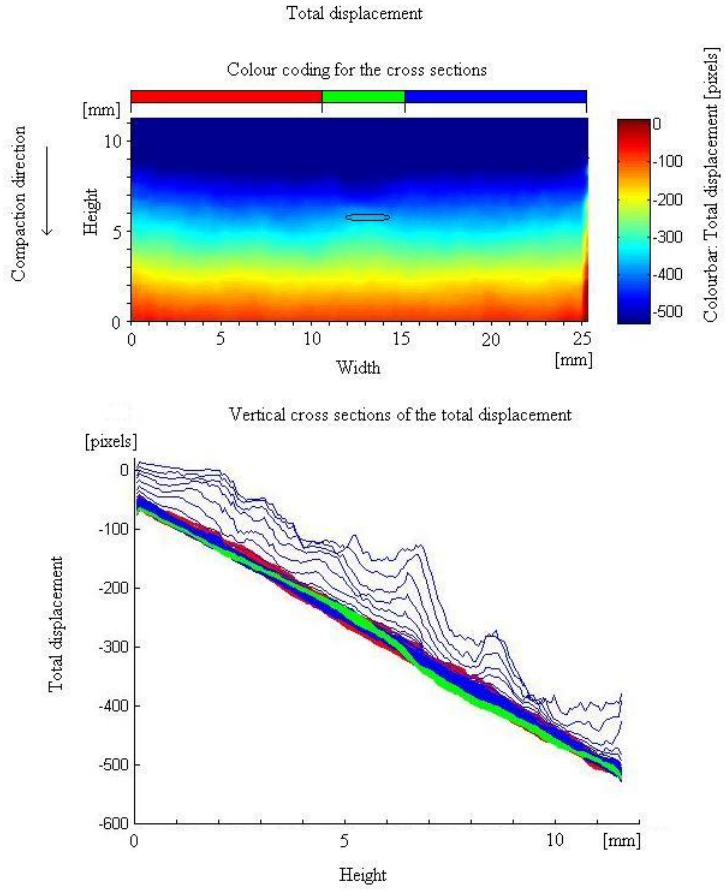

Figure 5.18: The upper plot is showing the total displacement of the soft inclusion experiment. The lower plot is showing cross sections of the total displacement field. The rough upper lines in the plot are cross sections taken to the right of 25 mm. What we see is the glass on the side of the cell. This area is over exposed by the camera and impossible to correlate so these lines are not of interest.

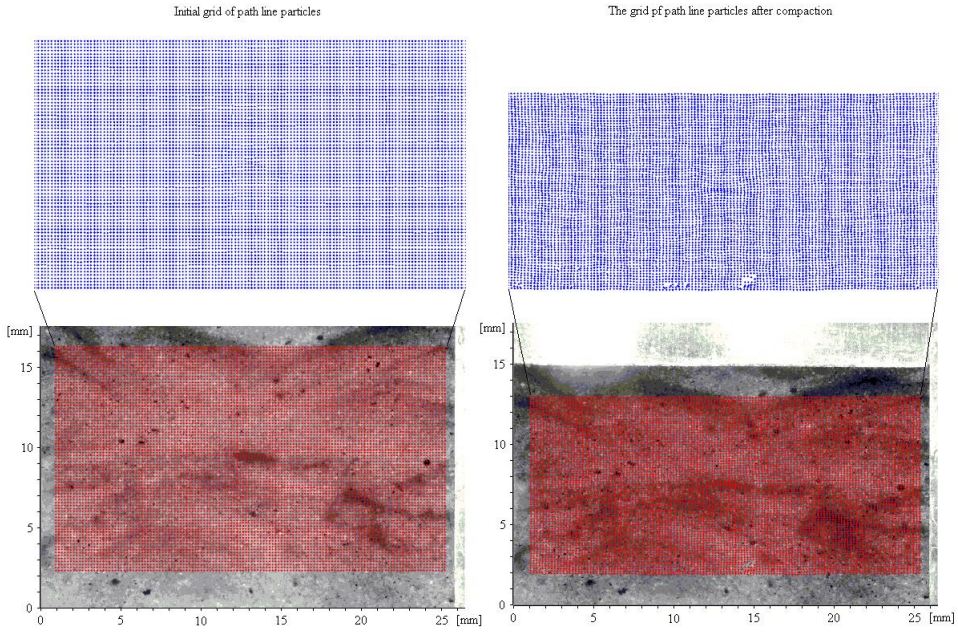

Figure 5.19: The grid of path line particles on top of the first and the final image.

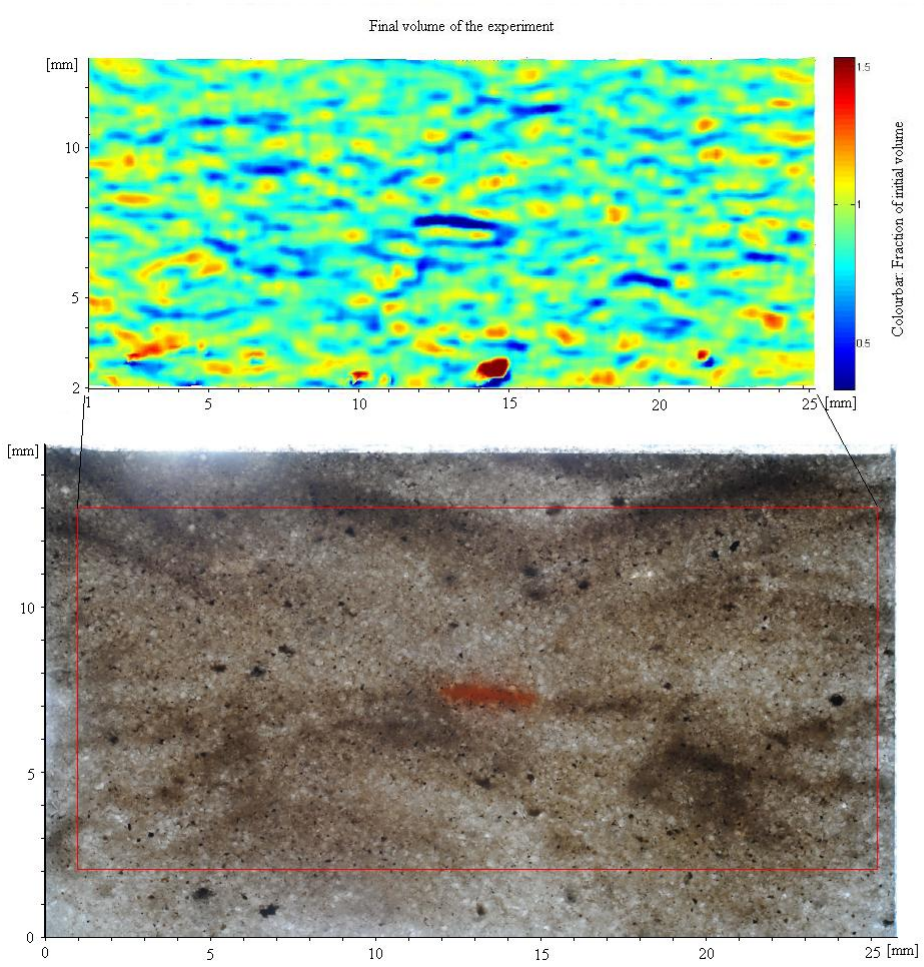

Figure 5.20: The final volume plot of the soft inclusion experiment. Under is the final image. We can see correlation between clay and compaction in some regions, but not everywhere.

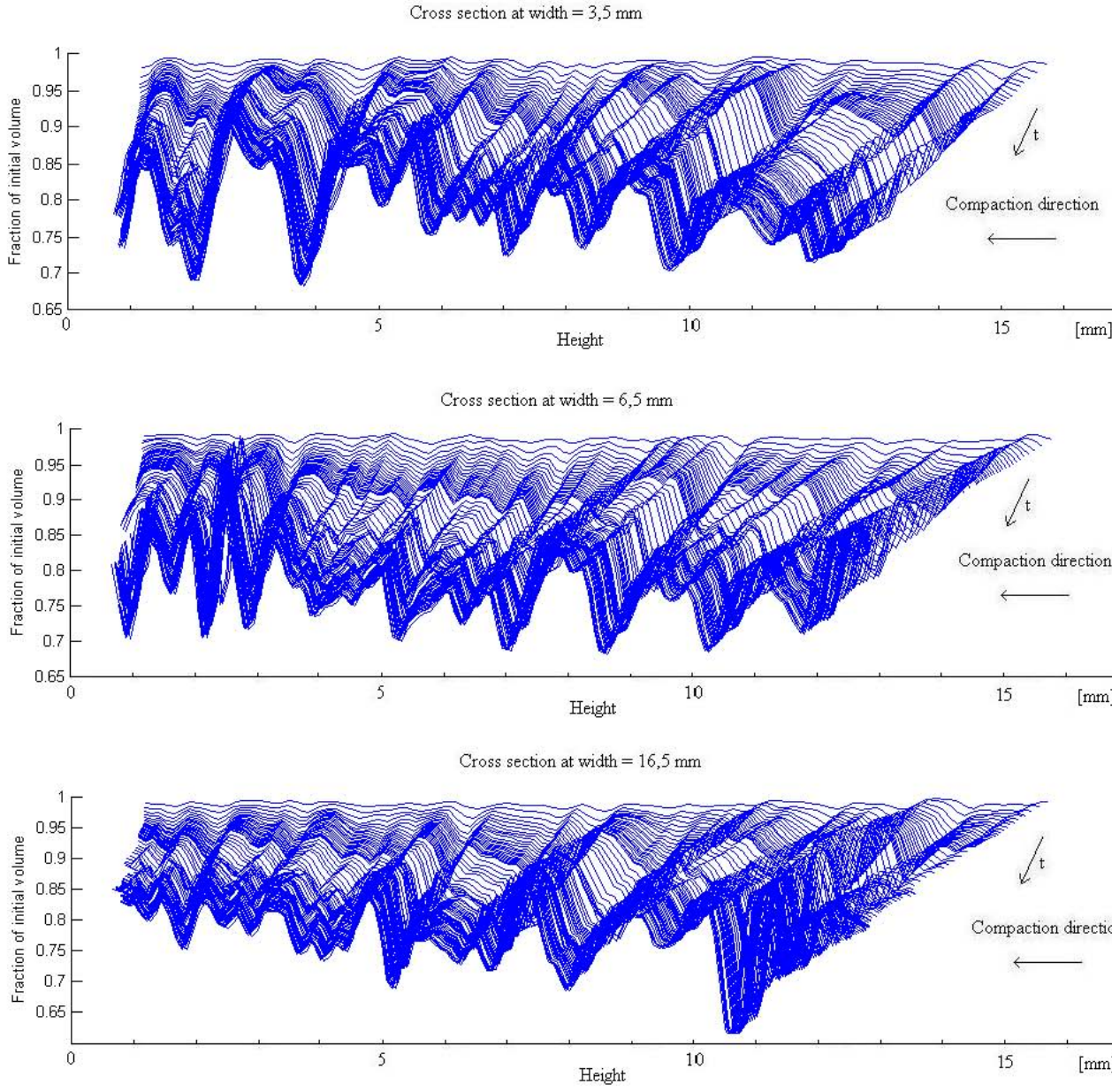

Figure 5.21: The time evolution of some cross section of the volume plot. We see that the final volume vary between 0,9 and 0,63. Meaning that the compaction vary between 10 and 37 percent.

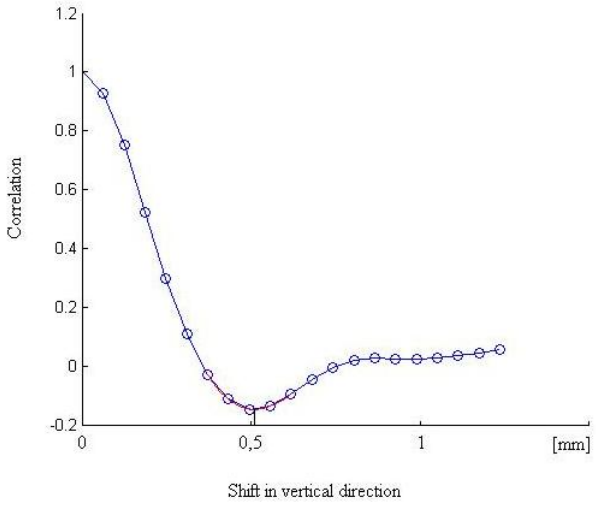

Figure 5.22: The autocorrelation is giving the spacing of the bands in the soft inclusion experiment.

The dominating spacing between the bands are 1,09 mm. This spacing is about half of the spacing in "hard inclusion 1".

We can also in this experiment see that the spacing is decreasing with the compaction of the system.

When we look at figure 5.26 and figure 5.27 we see that the difference is increasing through the whole compaction. Unlike in the "hard inclusion 1" experiment the difference is growing rapidly in the beginning before it slows down. It looks like it is growing with a constant rate 250 hours. We have also observed that the difference in compaction is close to logarithmic over time span of the experiment.

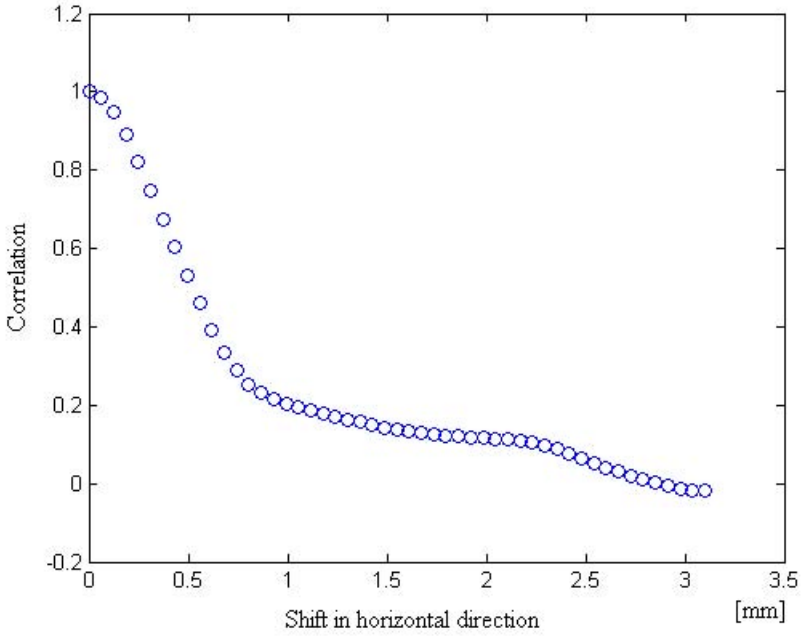

Figure 5.23: Horizontal autocorrelation of the final volume matrix. The function do not have a minimum point meaning that there are no repeating structures like bands in this direction. There is only a band structure lying in the horizontal direction.

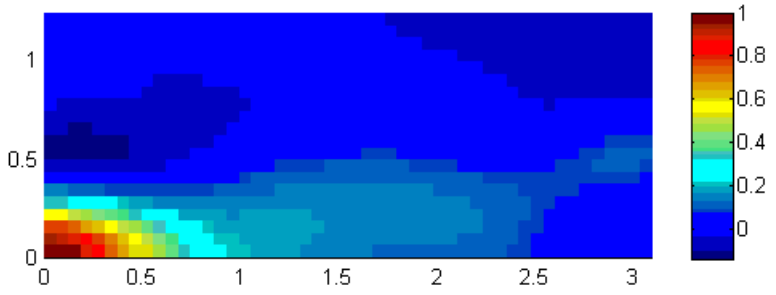

Figure 5.24: The correlation plane from the autocorrelation

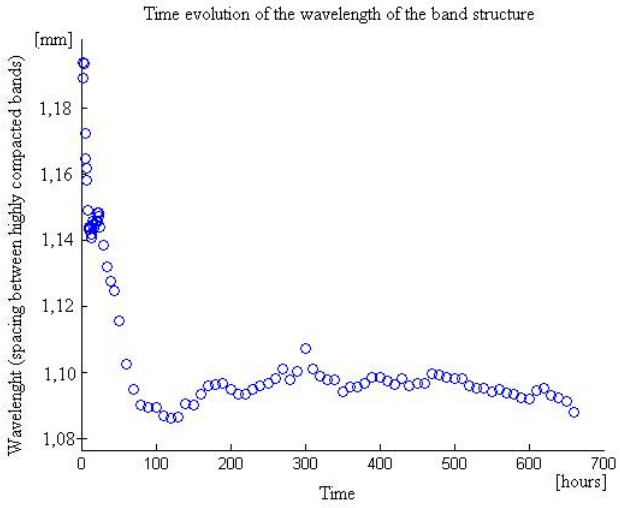

Figure 5.25: The autocorrelation gives the time evolution of the spacing in the soft inclusion experiment.

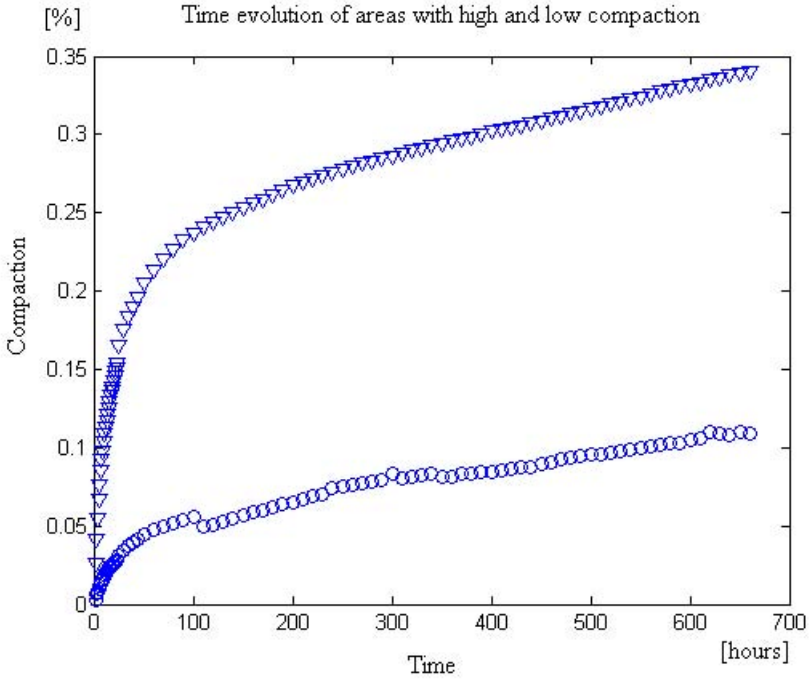

Figure 5.26: The plot shows the time evolution of the compaction in the areas with highest compaction and the areas with lowest compaction. We use the 1 percent with highest and the 1 percent with the lowest compaction values.

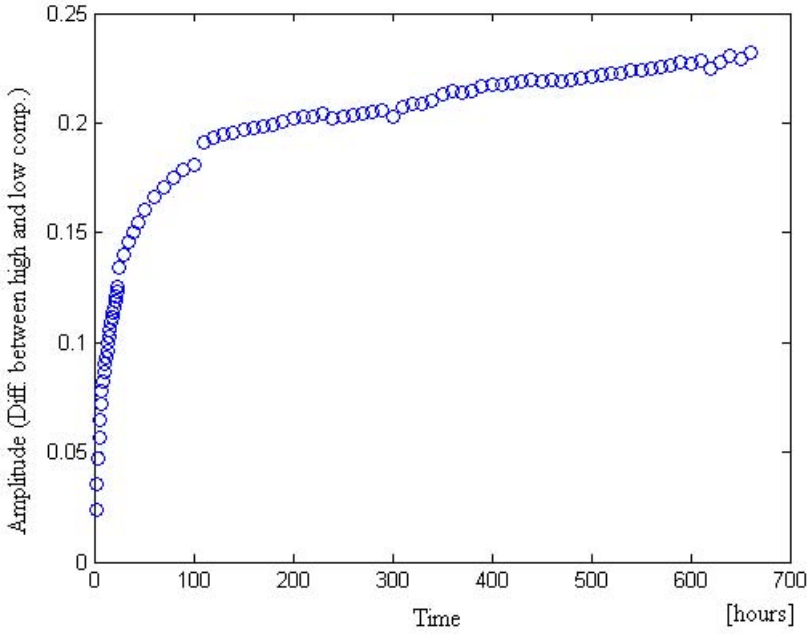

Figure 5.27: The plot shows the difference in compaction value between the highest and lowest compacted areas.

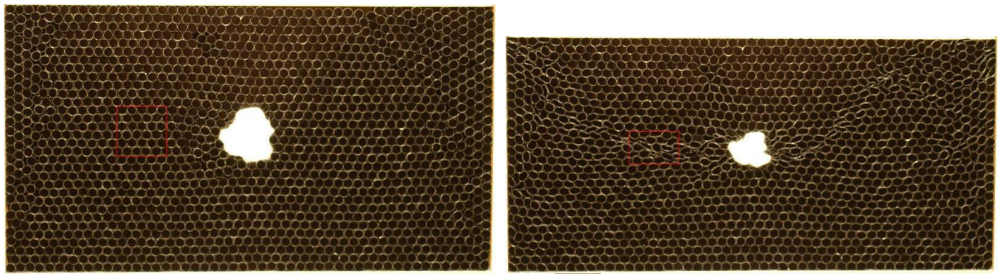

(a) (b)

Figure 5.28: (Drinking straw exp.). To the right is a photo before compaction. To the right is a photo in a late stage in the compaction. The red square is surrounding the same drinking straws in both photos. And so far in the compaction, is 48 percent of the total compaction localized inside the red square.

5.2 Drinking straw experiment

The photos from the drinking straw experiment are easier to analyse than the pictures from the salt experiment. The first analysis we did on these photos was to identify the cross sections of the drinking straws by threshold and then calculate the minor axis on each of them. When plotting the identified cross sections using minor axis as colour coding we get a nice visualization of where the deformation is localized (5.29). And we see a clear localisation of the deformation around the inclusion and in the upper corners of the cell. In the upper corners there are stress concentration because of wall friction and there are also stress concentrations on the sides of the soft inclusion. We see that these stress concentrations clearly causes localization of deformation.

In this experiment it is not hard to see the localization of deformation. But for the correlation method the photos from the powder compaction experiments are just as easy to correlate. So we wanted to use the same analysis on this experiment as a test of the analysis tool we had developed. In this experiment it is easy to see if the analysis is working properly because we can see the localization of deformation so clearly just by looking at the photos (see 5.28). The photos are going through the same correlation process as the powder compaction photos where we find displacement fields, strain fields,

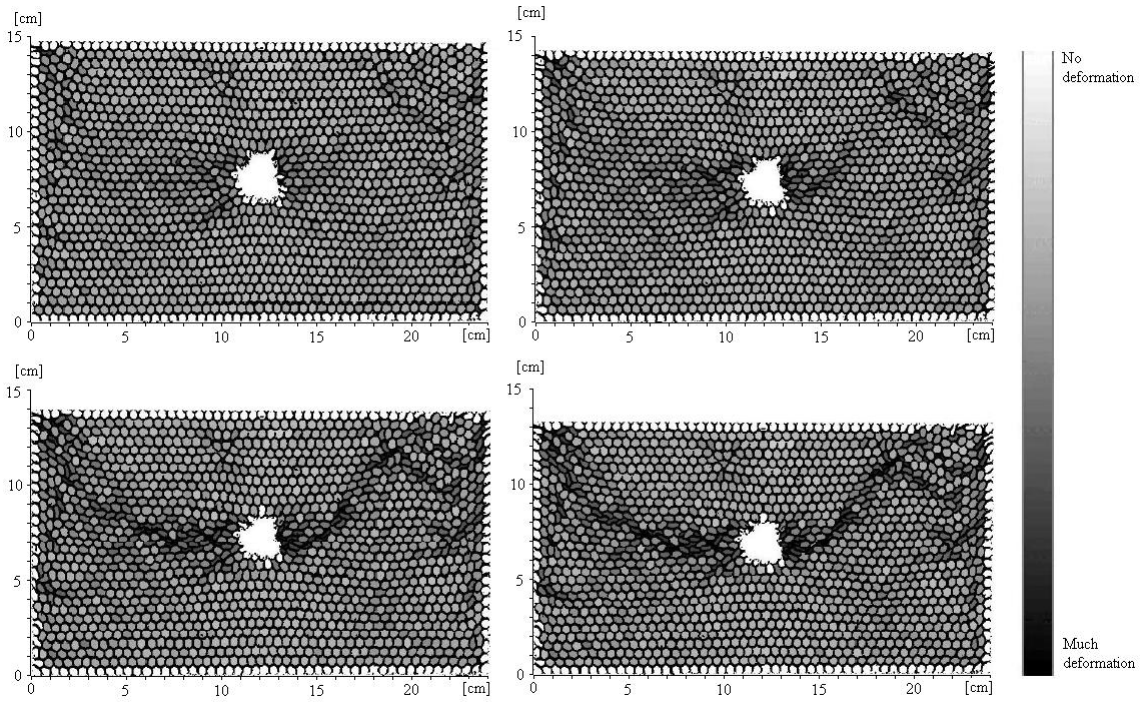

Figure 5.29: (Drinking straw exp.). Evolution of the compaction. The colour coding is the length of the minor axis of the elliptical shaped drinking straws. The dark straws are flat and much deformed. We can clearly see the dark line start around the inclusion and in the stress concentrations in the upper corners.

path lines and volume reduction.

We can clearly see from the plot of the total compaction (5.30) that the line of localized compaction is detected. We can also see the clear shift in slope in the cross sections in figure 5.30 indicating a localized compaction.

The path lines are also showing the same localization (5.31).

The field that shows the final volume also show a clear localization. We see that on the line of localization the volume is reduced to only 10 to 20 percent of the original volume.

The result from this experiment is a clear localisation of deformation that propagates from the inclusion and the areas with flaws in the packing and connects to a continuous line of localised deformation, an anticrack! It also a good test for the correlation method used on the powder compaction experiments. And the method seem to work very well. Both the displacement fields, strain fields, path lines and volume reduction seem to fit very well with the compaction we observe in the series of photos. It should not be easier to correlate the photos from the drinking straw experiment than the photos from the powder compaction experiments. This means that we can trust the results from the image analysis we do in the powder compaction experiment.

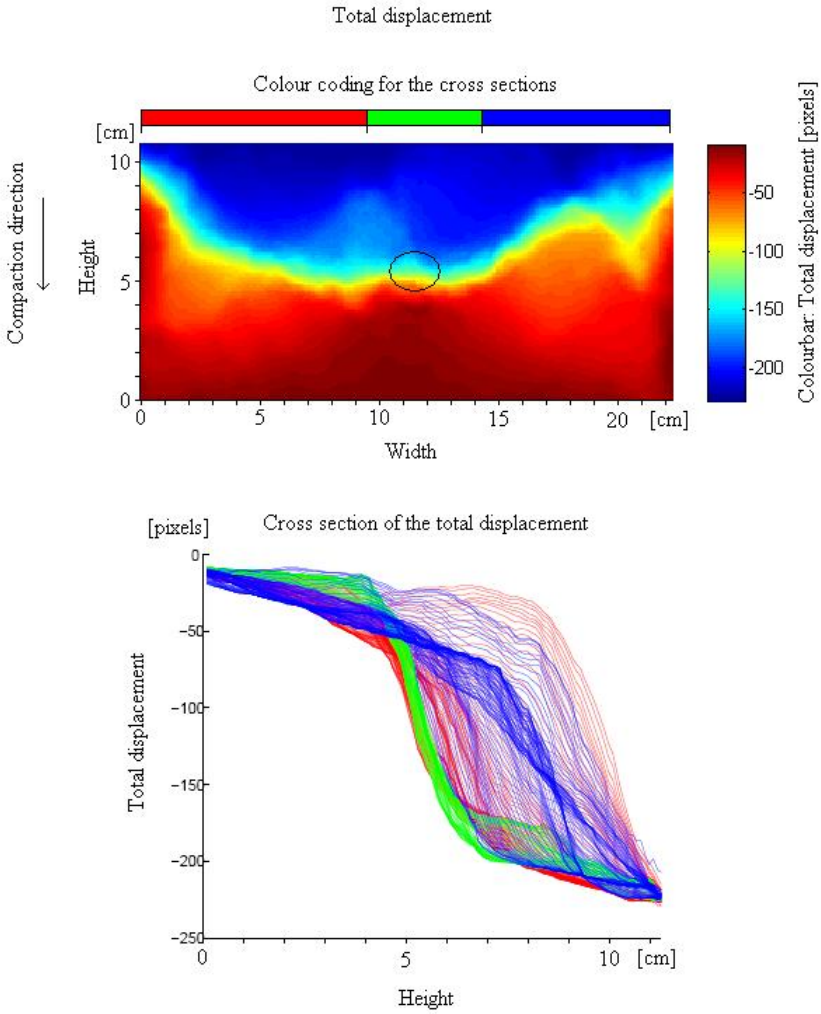

Figure 5.30: (Drinking straw exp.). To the left is the total compaction of the experiment. It is all the displacement fields added together. To the right is a plot of vertical cross sections. The x axis shows height (zero is the bottom of the cell. The y axis shows the displacement, a high negative number means much displacement.

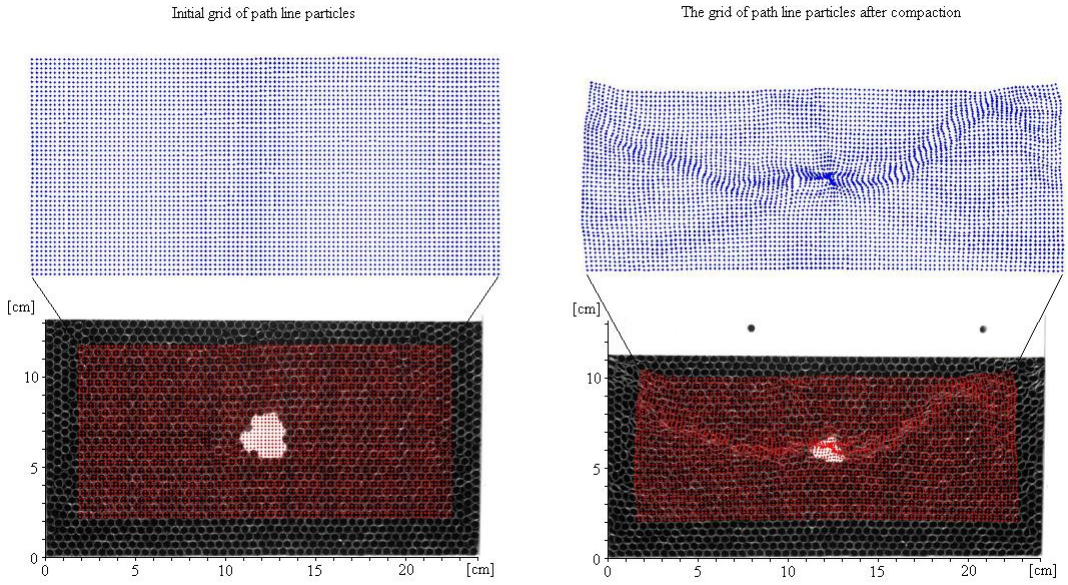

Figure 5.31: (Drinking straw exp.). Path lines following the particles through the compaction.

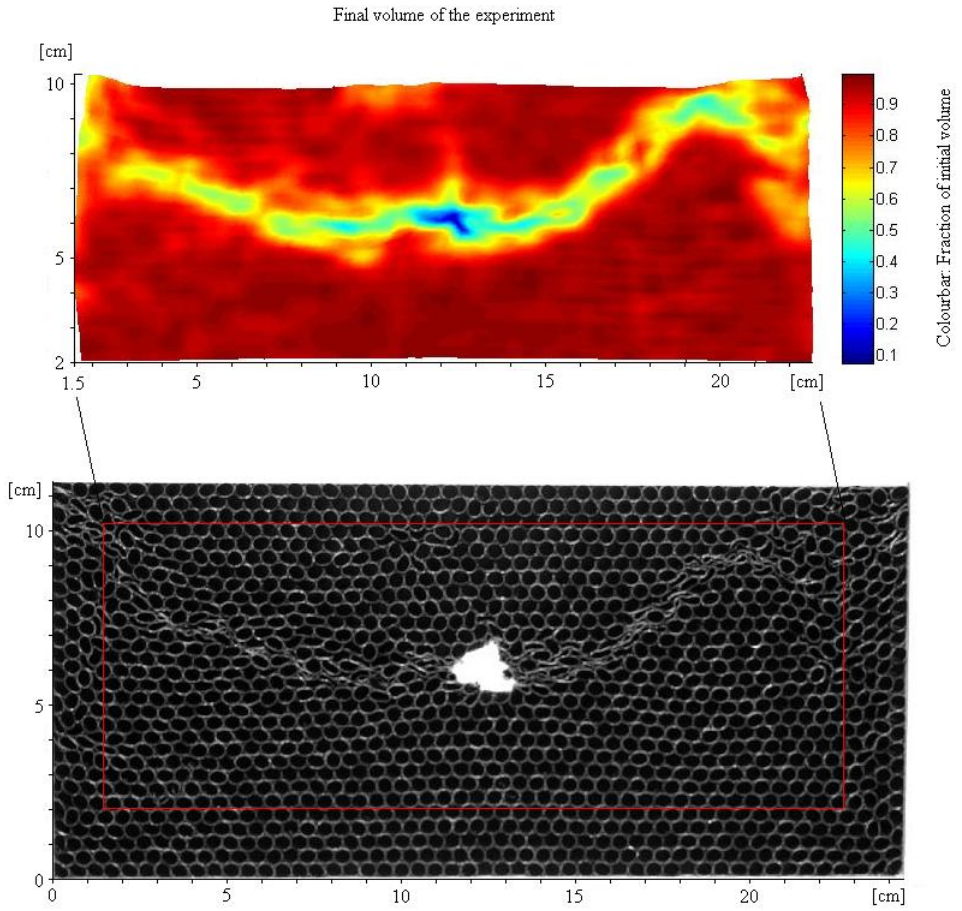

Figure 5.32: (Drinking straw exp.). Final volume field found by calculating the volumetric strain in the path line grid nodes for every time step.

5.3 Roughening experiment

The results from these experiments are the scanning files from the WLI. These files contain three dimensional data of the measured surface. This three dimensional set-up did not allow measurements during the experiment. But by comparing the before and after data we can see if there has been any roughening during the compaction. We compare the roughness measure R_q (RMS of deviation from mean height) before and after compaction for each surface. We did two experiments and one control experiment.

5.3.1 Roughening experiment 1

In this experiment we stack four polished sintered salt blocks on top of each other inside the glass cylinder filled with saturated fluid. Since clay is believed to be important in the formation of stylolites we put a thin layer of clay between the blocks. The blocks are stressed with a piston with a load of 4 kg. In the glass cylinder with inner diameter of 15 mm this gives a stress of 0,22MPa. The experiment is compacting for two month. The roughness of the blocks are measured before and after the compaction. We use 10 $\times$ magnification when we measure the samples. We can then measure an area of 635 $\times$ 478 micron. The interferometer have a stitching function that allows measurements with high magnification on areas bigger than the area covered by the objective. This require a special rig that is controlled by the interferometers software. This rig was not yet installed when this experiment was started so the measured areas are just 635 $\times$ 478 micron. We calculate R_q over the whole area and in a smaller section on each surface. There is some noise in the height field in the files from the interferometer. This noise are single pixels with very high or very low values and are distributed throughout the height field. This noise will increase the roughness (R_q). We remove this noise by using a median filter, and remove single pixels in areas with no successful measurement.

We can see that the roughness of all the surfaces have increased significantly.

5.3.2 Roughening experiment 2

In this experiment we have more variation in the set-up. We use five polished salt blocks that we stack in the glass cylinder. We have clay only on some of the surfaces this time. We also have salt powder with two different grain

Surface nr	R_q, whole area, (0,635×0,476 mm) before comp. [μm](*[nm])	R_q, whole area, (0,635×0,476 mm) after comp. [μm](*[nm])	R_q, section, (0,21×0,15 mm) before comp. [μm](*[nm])	R_q, section, (0,21×0,15 mm) after comp. [μm](*[nm])
1	1,03	7,66	243,39*	4,60
2	944,80*	6,04	285,36*	3,97
3	1,25	5,15	231,68*	4,26
4	6,52	10,63	1,87	6,30
5	1,26	6,66	686,56*	5,92
6	2,07	10,42	959,56*	5,7

Table 5.2: Rouhgness measured over the whole area and over a smaller section for each surface before and after compaction in roughening experiment 1. All the surfaces have had the same conditions during the compaction. They have all been pressed against another sintered block, and there has been a thin layer of clay between them.

sizes between some of the blocks. We use the same glass cylinder and 4 kg of weight on the piston. The cylinder is filled with saturated fluid. The set-up is sketched in figure 5.34. The rig for the stitching is now installed on the interferometer so we measure these surfaces with the same magnification as the last experiment (10×), but we stitch together different measurements to measure a larger area on the surfaces. We have time limitations so this experiment is only compacting for one month.The salt powder in this experiment is an attempt to create a jump in elastic properties which was the driving force in the model of Angheluta et al. [6].
Also in this experiment we remove noise using a median filter and removing single pixels.

The roughness have increased during the compaction for all the surfaces. Surface number 1 and 2 had cemented together so they broke in the attempt to take them apart. These surfaces had no clay between them. We see that surface 3 and 4 have a much higher R_q value than the rest of the surfaces when measured over the whole area. When measured over a smaller section the values are more similar. Surface 3 and 4 are two solid blocks pressed together while the rest of the surfaces in this experiment are pressed against salt powder. The R_q values measured in the smaller sections in this experiment can be compared with the R_q values measured over the whole area in Roughening experiment 1 since the area they are measured over fairly equal.

Surface nr	R_q, whole area, (7×7 mm) before comp. [μm]	R_q, whole area, (5×5 mm) after comp. [μm]	R_q, section, (1,2×1,2 mm) before comp. [μm]	R_q, section, (1,2×1,2 mm) after comp. [μm])
1	-	-	-	-
2	-	-	-	-
3	4,60	17,35	1,55	7,13
4	4,87	22,67	4,03	7,00
5	5,05	11,18	1,60	4,86
6	2,74	12,60	1,02	8,57
7	2,28	7,87	1,31	5,23
8	2,51	4,87	1,46	3,32

Table 5.3: Rouhgness measured over the whole area and over a smaller section for each surface before and after compaction for roughening experiment 2. The surfaces have had different condition during the compaction, see figure 5.34

We see that these values are comparable. When we look at all the surfaces that have been pressed against another solid block with clay in between, they are all giving roughnesses of the same sizes when measured over a small area. When we look at the two measurements that are made over a bigger area we see a much higher R_q value. This might indicate that the roughening is on a length scale longer than the size of the smaller sections we measure over. When we look closer at surface 3 and 4 we see a peak to peak length in the range 2-4 mm.

5.3.3 Roughening control experiment

We wanted to see if the blocks got a rougher surface when lying in saturated fluid without an applied stress. We stack two polished block on top of each other in the glass cylinder, but we do not apply a piston with a dead weight. This experiment is running for one month.

We also in this experiment see an increase in roughness. When we look at the R_q values measured over the whole area, they are comparable with the R_q values of surface 5 and 6. These surfaces have been pressed against coarse grained salt powder. Surface 7 and 8 are less rough than the control exper-

Surface nr	R_q, whole area, (7×7 mm) before comp. [μm]	R_q, whole area, (5×5 mm) after comp. [μm]	R_q, section, (1,2×1,2 mm) before comp. [μm]	R_q, section, (1,2×1,2 mm) after comp. [μm])
1	4,65	12,15	1,80	9,95
2	2,39	12,65	1,21	8,80

Table 5.4: Rouhgness measured over the whole area and over a smaller section for each surface before and after compaction for roughening control experiment. The blocks are just resting on top of each other. There is no stress and no clay present.

iment, they have been pressed against fine grained salt powder. Measured over a small area the control experiment are giving the roughest surfaces.

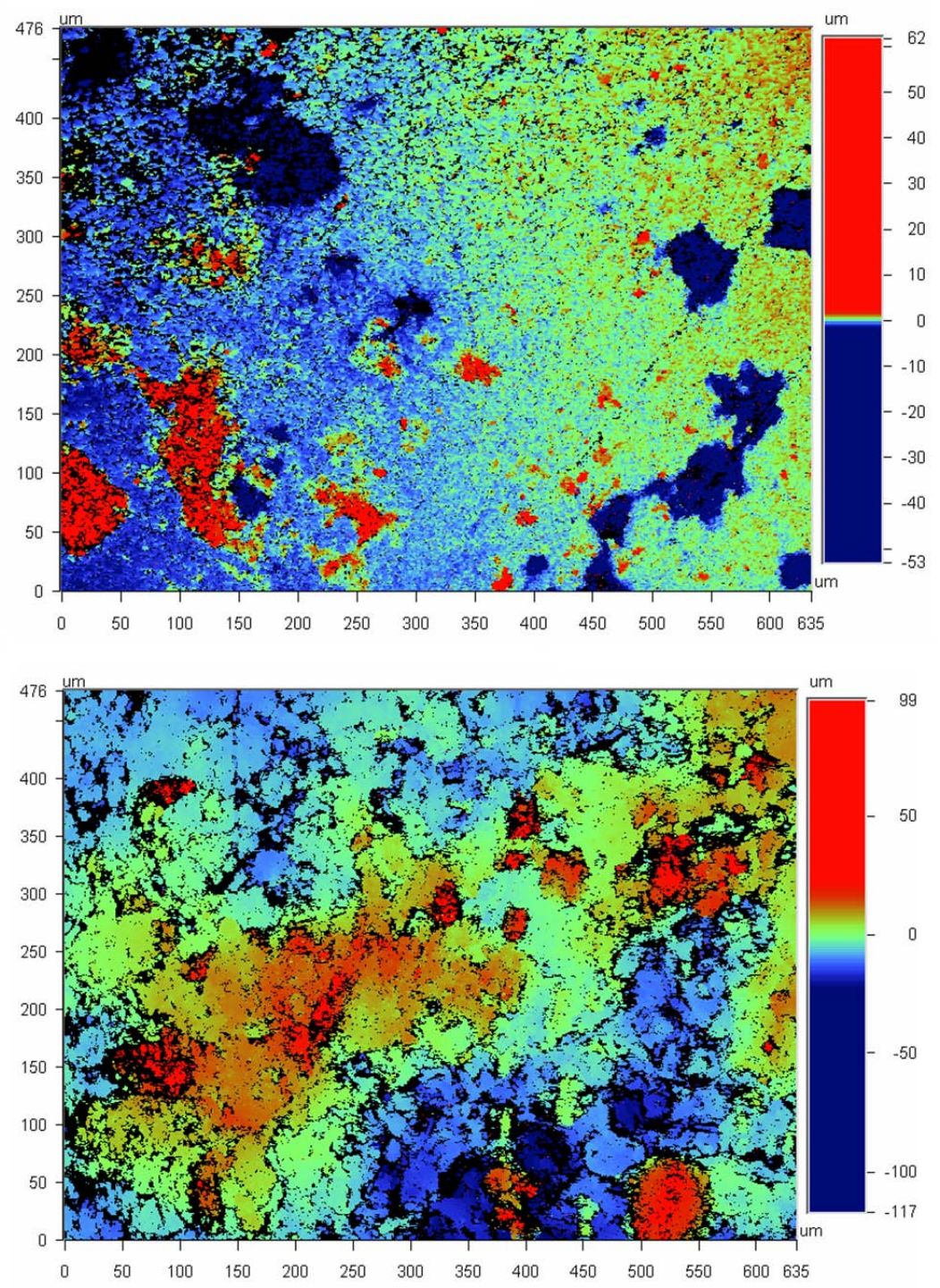

Figure 5.33: The upper figure is the height profile of a surface before compaction measured with the interferometer. The lower is the same surface after compaction. This is a measurement measured over a area of 0,635×0,476 mm.

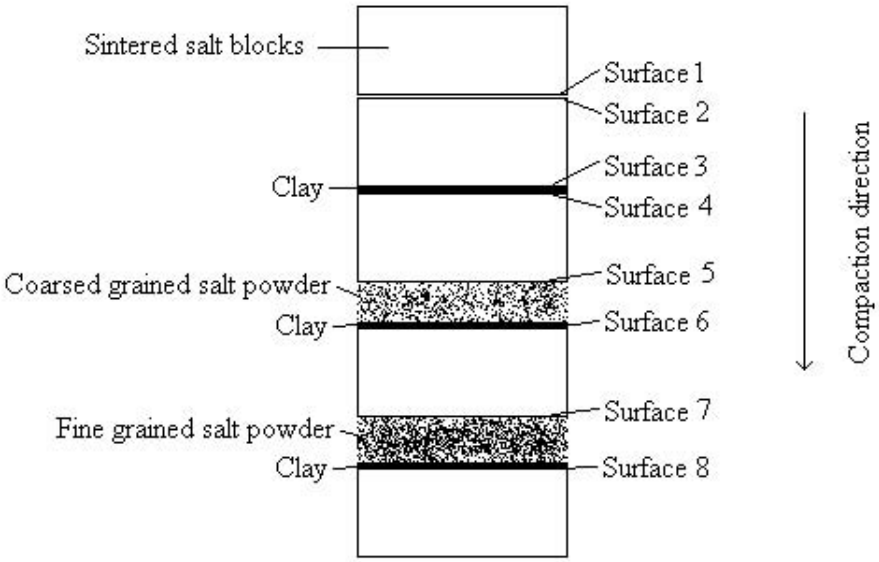

Figure 5.34: Sketch of the different surfaces and what they are pressed against.

5.4 Discussion

5.4.1 Powder compaction

In this experiment we wanted to see the evolution of compaction of a porous sedimented material around an inclusion. The anticrack model where stress concentrations around the inclusion are causing localized compaction was one of the central theories we wanted to link this experiment to. We did three experiments with this set-up, two with a hard inclusion and one with a soft inclusion. Neither of these experiments show any sign of localized compaction around the inclusion. The inclusion does not seem to affect the compaction at all. When we did the experiment with the drinking straws we clearly got an anticrack with its origin in the soft inclusion, but in the powder compaction experiments nothing happens around the inclusion. What we do see in the powder compaction experiments are band structures lying normal to the compaction direction. So the compaction is not homogeneous. The compaction in the band structure vary between 8 and 28 percent. The total compaction of the experiments are 16,5 in "hard inclusion 1" and 21,5 percent in "soft inclusion". By weighing the salt we pour in to the cell and measure the starting height of the salt column in the cell we can calculate the starting porosity when we know the density of NaCl. The starting porosity of the experiments are about 25 percent. Our analysis of the compaction shows a local compaction of up to 37 percent. If our analysis and initial porosity measurement are correct, this means that some of the dissolved material has been transported out of the local area with high compaction and precipitated in a region with lower local compaction, or that there was local porosity variations in the salt when the compaction started.
The band structures we observe in the experiments have wavelengths of 2,20 mm ("hard inclusion 1") and 1,09 mm ("soft inclusion"). So what is triggering this localization of compaction, and why is there a spacing of 1-2 mm? We can clearly see that the inclusions do not trigger the localization. Variation in clay concentration is one possibility. Clay is known to speed up the strain rate in compacting salt. It is hard to see from the images in "hard inclusion 1", but in the images from "soft inclusion" where the light is shining through the sample we can see that there is a small correlation between clay concentration and compaction in some regions (see figure 5.20). So clay might be a triggering factor for localized compaction, but where does the dissolved material precipitate? If it precipitates in the local pore space, the faster compaction triggered by the clay will slow down again because the stress in the grain contacts is decreasing with lower porosity. If some of the dissolved material is diffusing further than the distance out in the local

pore space the porosity will decrease less, and the effect of the increasing clay concentration as the material compacts might be bigger than the effect of decreasing porosity. If the effect of increasing clay concentration is bigger than the effect of decreasing stress because of decreasing porosity the localization will speed up. This requires that some material is diffusing farther than out in the local pore space. The characteristic diffusion length in a system depend on many parameters. Temperature, precipitation rate and the diffusion constant are some of them. Is the spacing we see in the band structure linked to the characteristic diffusion length in the system? And can the light-set-up we used in "hard inclusion 1", which radiated a lot of heat, be a reason for a bigger wavelength of the band structure in this experiment? Higher temperature will increase the characteristic diffusion length. The fact that the cell is heated on one side and that it therefore is a temperature gradient in the cell can also be a driving force for the diffusion. We have not calculated an estimate for this length, but we may compare our results to stylolite spacing in nature. The spacing of stylolites in calcitic rocks are in the range 1-5 cm. The characteristic diffusion length, Δl, in a system is proportional to the square root of the diffusion coefficient,D, times the expected time ,Δt, it take for dissolved material to precipitate, $\Delta l \approx \sqrt{2D\Delta t}$. Δt is proportional to one over the precipitation rate, γ; $\Delta t \approx \frac{1}{\gamma}$. This gives us that Δl is proportional to the square root of D over γ; $\Delta l \approx \sqrt{\frac{2D}{\gamma}}$. The dimensions here are: $[D] = \frac{m^2}{s}$ and $[\gamma] = \frac{1}{s}$. Dissolution rates and precipitation rates may in general be different due to impurities that inhibit precipitation more than dissolution. On the other hand, in order to get an idea of the relative precipitation rates of calcite and halite we will refer to studies of dissolution of the two minerals at very high stirring rates where the effects of diffusion are minimized [5, 7]. The ratio of dissolution rates $\gamma_{\text{halite}}/\gamma_{\text{calcite}}$ are between $3.5 \cdot 10^4$ and $5.3 \cdot 10^5$. Our simple dimensional analysis states that the square root of this ratio enters the ratio of diffusion lengths. Consequently, our observations of wavelength of banding in NaCl of 1-2 mm corresponds to nucleation of stylolites in calcitic rocks at distances of 20 cm to 1.5 m. Considering that stylolites will approach each other (sometimes by more than 10 cm) as material is dissolved on the stylolite surfaces, our crude estimate hits the nail surprisingly well. We may therefore claim that these experiments possibly represent an experimental demonstration of nucleation of stylolite planes.

Merino et al. [16] suggests that a long characteristic diffusion length is causing initially more porous areas to get even more porous because of higher stress in grain contacts and a long characteristic diffusion length. They suggest that this increasing porosity will end in a collapse of the material and

that this is the origin of localisation features like stylolites.
Another possible consequence of a initial high local porosity is that instead of increasing the porosity, this volume preserves its porosity by compacting faster. This will lead to a higher concentration of insoluble particles like clay that again will increase the dissolution. In a natural system can areas with higher porosity act as pathways for fluid flow that again will transport dissolved material away from the dissolution site.

5.4.2 Drinking straw experiment

The compaction in this experiment was purely mechanical. It compacted because of bending of the elastic drinking straws, and later in the compaction the drinking straws collapse in highly stressed regions. We can clearly see an anticrack in this experiment. There is a band of localized compaction propagating out from the inclusion. This band is meeting up with the bands nucleated in the stress concentrations in the upper corners. The three areas that should have the highest stress in the cell are the top corners (because of wall friction) and the areas next to the inclusion. It is exactly in these areas the compaction is localized. The packing of the straws are regular and close to a triangular close pack.

5.4.3 Roughening experiment

We measured the roughness of a number of surfaces before and after compaction. All the surfaces get rougher after compaction, including the control experiment where there was no applied stress. If we compare the roughness of the different experiments with the control experiment we see that the control experiment gives the roughest surfaces when measured over smaller areas. This probably has something to do with the roughening process in the non stressed blocks in the control experiment. The blocks are polished, so the grains on the surface have all a planar surface with a normal vector pointing in the same direction. The crystal lattice direction of the surface grains are though not the same for all the grains. This will lead to crystal growth on grains with a certain lattice direction compared with the polished direction. The lengthwise of the roughness is then on grain size scale.
The roughening process in the stressed blocks might be totally different and have totally different length scale. The R_q values measured over a large area are smaller or equal to the control experiment for the blocks pressed against salt powder. So the stress applied does not increase the roughness compared with the control experiment when a solid block is pressed against powder. When two solid blocks are pressed together we get a large R_q value when

measured over a large area. This might indicate that the length scale of the roughness is bigger than the length of the smaller areas we measure over (bigger than ∼1mm). The only R_q values bigger than those for the control experiment are the values measured over a large area of surface 3 and 4 from roughening experiment 2. These surfaces are pressed against solid blocks with a thin layer of clay. We may speculate that the stress transmission between two sintered blocks allows the development of larger scale structures than when powder is involved.

5.5 Conclusion

We have studied both systems with mechanical compaction and systems with chemical compaction in this study. In the mechanically compacted system we compacted drinking straws in a regular packing around a soft inclusion. this experiment showed a clear localization of compaction around the inclusion. There was an anticrack forming that propagated out from the inclusion. In our powder compaction experiment we studied a system of compacting non cemented salt powder around an inclusion. By non cemented we mean that the grains where not cemented together when the compaction began. The inclusion did not affect the compaction of the salt. There was no localization of compaction around the inclusion and no anticracks forming. Soft and hard inclusion have no effect on the compaction of a non cemented granular systems compacting by pressure solution. If stylolites form in non cemented sediments, localization of compaction does not occur by an anticrack spreading. The granular system compacted by pressure solution develops a periodic "compaction band" structure oriented normal to the compaction direction. The spacing of these bands are 1-2 mm. This is consistent with the stylolite spacing observed in calcitic rocks assuming that the precipitation rate determines the characteristic diffusion length. We propose that the mechanism for instability causing localization of compaction is initial porosity variations and/or variations in clay concentration.
The roughness of the surfaces in the roughening experiment only show a roughness larger than the unstressed control experiment when measured over a big area. This indicates that the surfaces roughen at a length scale bigger than $\sim 1mm$. When we measure peak to peak lengths on the surfaces we get a wavelength of 2-4 mm.

5.6 Future work

We believe it is very important for the further study of stylolites to concentrate on precipitation and diffusion lengths. What we missed in our powder compaction experiment was a porosity field. If there is possible to map the compaction and the porosity evolution of a system one would get information about where things precipitated. We believe this is the key to further development in the stylolite study.

Appendix A

Matlab code

Running the correlation code.

```
clear

%IMPATH = './Data/'; % Image folder
imname = 'Liten_'; % image file name
imext  = 'tif'; % Image file-extension
%
%
% NUM PARAMETERS
BWTH         = 40; % Test box width +/-
SRNG1        = [-50, 5]; % Search range   +/-
SRNG2        = [-20,20];

% LOAD IMAGE 1
fname = [imname,num2str(1,'%02d'),'.',imext];
IM1    = imread(fname,imext);\\


IM1    = rgb2gray(IM1);
IM1    = flipud(im2double(IM1));
[IM1] = cleanImageStd(IM1);

[N1,N2] = size(IM1);

stp  = 10;
ind1 = (BWTH-SRNG1(1)+1):stp:(N1-BWTH-SRNG1(2));
ind2 = (BWTH-SRNG2(1)+1):stp:(N2-BWTH-SRNG2(2));
```

```
for n = 1:23
    fname = [imname,num2str(n+1,'%02d'),'.',imext];
    IM2    = imread(fname,imext);
    IM2    = rgb2gray(IM2);
    IM2    = flipud(im2double(IM2));
    [IM2] = cleanImageStd(IM2);

    u    = zeros(numel(ind1),numel(ind2));
    v    = zeros(numel(ind1),numel(ind2));

    cnt1 = 0;
    for R1 = ind1
        cnt1 = cnt1 + 1;
        cnt2 = 0;
        %tic
        for R2 = ind2
            cnt2 = cnt2 + 1;
            [r1,r2,rmat_min] = DigitalImageCorrelation ...
                                (IM1,IM2,R1,R2,BWTH,SRNG1,SRNG2);
            v(cnt1,cnt2) = r1-R1;
            u(cnt1,cnt2) = r2-R2;
        end
        %toc
    end

    % SAVE DATA
    save(['displacement_liten_BWTH_',num2str(BWTH), ...
     '_',num2str(n,'%02d')],'u','v')

    IM1 = IM2;
end
```

The correlation code.

```
function [r1,r2,rmat_min] = DigitalImageCorrelation ...
(IM1,IM2,R1,R2,BWTH,SRNG1,SRNG2)
%
% PERFORMES AN IMAGE CORRELATION BETWEEN IMAGES IM1 AND IM2.
% R1 AND R2 IS THE INITIAL CENTER FOR THE CORRELATION
% BWTH : IS THE BIN WIDTH
% SRNGX AND SRNGY : SEARCH GRID
%
% NOTE: Similar to 'DigitalImageCorrelation' but
% uses a steepest descent
%       method to find the minimum.
%


r1 = R1;
r2 = R2;

% SIZE OF CORRELATION MAP
ind  = -BWTH:BWTH; % relative box index list

%%%%%%%%%%%%%%%%%%%%%%%%%%%%%%% CORRELATION RUTINE

i1 = round(r1);
i2 = round(r2);

% LOCAL MATRIX
IM11 = IM1(i1+ind,i2+ind);

rval_min = realmax;

%---------------------------- Coars minimums search
for n1 = 1:1:20
    for n2 = 1:1:20

        % POSITIONS TO BE CORRELATED
        rct1 = i1 + round( n1*(SRNG1(end)-SRNG1(1))/21 ) ..,
         + SRNG1(1);
        rct2 = i2 + round( n2*(SRNG2(end)-SRNG2(1))/21 ) ...
         + SRNG2(1);
```

```
        IM12 = IM2((rct1)+ind, (rct2)+ind);


        % CORRELATION VALUE
        rval                            = 1 - sum(IM11(:).*IM12(:))/sqrt(sum(IM11

        if rval < rval_min
            rc1      = rct1;
            rc2      = rct2;
            rval_min = rval;
        end

    end
end

%---------------------------------------- Steepest decent
is_min = false;
while ~is_min
    is_min = true;
    for n1 = -1:1
        for n2 = -1:1
            % POSITIONS TO BE CORRELATED
            rct1 = rc1 + n1;
            rct2 = rc2 + n2;


            IM12 = IM2((rct1)+ind, (rct2)+ind);

            % CORRELATION VALUE
            rval                            = 1 - sum(IM11(:).*IM12(:))/sqrt(sum(
            if rval < rval_min

                drc1     = n1;
                drc2     = n2;
                rval_min = rval;
                is_min   = false;
            end

        end
```

```
    end
    if ~is_min
        rc1 = rc1 + drc1;
        rc2 = rc2 + drc2;
    end
end
%%%%%%%%%%%%%%%%%%%%%%%%%%%%%%%%%%%%%%%%%%%%%%%%%%%%%%%%%%%%%%%%%%%


%%%%%%%%%%%%%%%%%%%%%%%%%%%%%%%%%%%% SUB PIXEL RESOLUTION
% Find min
m1 = rc1;
m2 = rc2;

% BOX PARABOLA FIT
bpf1 = (-1:1);
bpf2 = (-1:1);

% SUB PIXEL RESOLUTION SCHEME
% calculate z
z = zeros(3,3);
for n1 = -1:1
    for n2 = -1:1
        % POSITIONS TO BE CORRELATED
        rct1 = rc1 + n1;
        rct2 = rc2 + n2;


        IM12 = IM2((rct1)+ind, (rct2)+ind);

        % CORRELATION VALUE
        z(n1+2,n2+2) = 1 - sum(IM11(:).*IM12(:))/sqrt ...  (sum(IM11(:).^2))/sqr
    end
end

bpf2m = repmat(bpf2 ,3,1);
bpf1m = repmat(bpf1',1,3);

% FIT THE 3 X 3 REGION AROUND THE MIN
%OF THE CORRELATION MATRIX r TO A PARABOLA
[a_fit,z_fit] = fit_parabola(bpf2m,bpf1m,z);
```

```
[uloc,vloc]   = find_displacement(a_fit);

% RECOGNIZED MATERIAL POINT IN IMAGE 2
r1            = (R1-i1) + m1 + vloc;
r2            = (R2-i2) + m2 + uloc;


%%%%%%%%%%%%%%%%%%%%%%%%%%%%%%%%%%%%%%%%%%%%%%%%%%%%

%%%%%%%%%%%%%%%%%%%%%%%%%%%%%%%%%%%% rmat_min
rmat_min = abs(IM11 - IM12);
```

Finding displacement.

```
function [u,v] = find_displacement(a)


A = [2*a(1), a(3);
     a(3), 2*a(2)];

b = [-a(4); -a(5)];

x = A \ b;

u = x(1);
v = x(2);
```

Fitting parabola.

```
function [a_fit, z_fit] = fit_parabola(x,y,z)

nel = numel(x);
A = [reshape(x.^2,nel,1), reshape(y.^2,nel,1), reshape ...
(x.*y,nel,1), reshape(x,nel,1), reshape(y,nel,1), ones(nel,1)];

b = reshape(z,nel,1);

a_fit = A \ b;
z_fit = reshape(A*a_fit, size(z));
```

Cleaning images.

```
unction [imc] = cleanImageStd(im)
%
% Removes intermediate values from the image
%
% Input: im  : grayscale image
%        std :

[N1,N2] = size(im);
ind     = -25:25;
imc     = zeros(size(im));
onest   = ones(1,numel(ind)^2);
iml     = ones(numel(ind)^2,1);

display('NOISE REMOVAL')
tic
for n1 = 26:N1-max(ind)
    for n2 = 26:N2-max(ind)

        iml(:) = im(n1+ind,n2+ind);
        mn  = onest*iml/numel(iml);


        sd  = sqrt((iml-mn)'*(iml-mn)/numel(iml));
        lb  = mn-sd;
        ub  = mn+sd;
        imc(n1,n2) = (im(n1,n2) < lb)*(im(n1,n2)-lb) ...
          + (im(n1,n2) > ub)*(im(n1,n2)-ub);
    end
end
toc
```

Bibliography

[1]

[2]

[3]

[4] Einat Aharonov and Regina Katsman, Mechanisms of stylolite formation: insights from modeling.

[5] Marwan Alkattan, Erik H. Oelkers, Jean-Louis Danduand, and Jacques Schott, Experimental studies of halite dissolution kinetics, 1 the effect of saturation state and the presence of trace metals, Chemical Geology **137** (1997), 201–219.

[6] L. Angheluta, E. Jettestuen, J. Mathiesen, F. Renard, and B. Jamtveit, Stress-driven transformation and the roughening of solid-solid interfaces, Physical Review Letters **100** (2008), no. 096105.

[7] R. G. Compton and K. L. Pritchard, The dissolution of calcite at ph>7: Kinetics and mechanism, Philosophical Transactions of the Royal Society of London. Series A, Mathematical and Physical Sciences (1990).

[8] Renard F. and Dysthe D. K., In encyclopedia of sediments and sedimentary rocks, Kluwer academic publishers, 2003.

[9] Raymond C. Fletcher and David D. Pollard, Anticrack model for pressure solution surfaces, Geology **9** (1981), 419–424.

[10] Frank Fueten, Pierre-Yves F. Robin, and Michael Schweinberger, Finite element modelling of the evolution of pressure solution cleavage, Journal of Structural Geology **24** (2002), 1055–1064.

[11] Doron Gal, Amos Nur, and Einat Aharonov, Stability analysis of a pressure-solution surface, Geophysical Research Letters **25** (1998), no. 8, 1237–1240.

[12] Milton T. Heald, Stylolites in sandstone, Journal of Geology **63** (1955), no. 2, 101–114.

[13] Po-Chih Hung and A. S. Voloshin, In-plane strain measurement by digital image correlation, J. of the Braz. Soc. of Mech. Sci. Eng. (2003), no. 3.

[14] R. Katsman, E. Aharonov, and H. Scher, Localized compaction in rocks: Eshelby's inclusion and the spring network model, Geophysical Reasurch Letters **33** (2006), no. L10311.

[15] Daniel Koehn, Francois Renard, Renaud Toussaint, and Cees W. Passchier, Growth of stylolite teeth patterns depending on normal stress and finite compaction, Earth and Planetary Science Letters **257** (2007), 582–595.

[16] Enrique Merino, Peter Ortoleva, and Peter Strickholm, Generation of evenly-spaced pressure-solution seams during (late) diagnesis: A kinetic theory, Contibutions to Mineralogy and Petrology **82** (1983), 360–370.

[17] Won C. Park and Erik H. Schot, Stylolites: Their nature and origin, Journal of Sedimentary Petrology **38** (1968), no. 1, 175–191.

[18] C. Poirier, M. Ammi, D. Bideau, and J.P. Troadec, Experimental study of the geometrical effect in the localization of deformation, Physical Review Letters **68** (1992), no. 2.

[19] Francois Renard, Dag Dysthe, Jens Feder, Knut Bjørlykke, and Bjørn Jamtveit, Enhanced pressure solution creep rates induced by clay particles: Experimental evidence in salt aggregates, Geophysical Research Letters **28** (2001), no. 7, 1295–1298.

[20] Francois Renard, Jean Schmittbuhl, Jean-Pierre Gratier, Paul Meakin, and Enrique Merino, Three dimensional roughness of stylolites in limestone, Journal of Geophysical Research **109** (2004), no. B03209.

[21] D. J. Srolovitz, On the stability of surfaces of stressed solids, Acta Metall **37** (1989), no. 2, 621–625.

[22] Peter K. Weyl, Pressure solution and the force of crystallization-a phenomenological theory, Journal of Geophysical Research **64** (1959), no. 11.